12-2004

Trade Space Analysis of Antenna Array Architecture Using System Modeling Tools

Eugene Johnson

TRADE SPACE ANALYSIS OF ANTENNA ARRAY ARCHITECTURE USING SYSTEM MODELING TOOLS

THESIS

Eugene Johnson, 1Lt, USAF
AFIT/GE/ENG/04-26

DEPARTMENT OF THE AIR FORCE
AIR UNIVERSITY
AIR FORCE INSTITUTE OF TECHNOLOGY

Wright-Patterson Air Force Base, Ohio

The views expressed in this thesis are those of the author and do not reflect the official policy or position of the United States Air Force, Department of Defense, or United States Government.

AFIT/GE/ENG/04-26

TRADE SPACE ANALYSIS OF ANTENNA ARRAY ARCHITECTURE USING SYSTEM MODELING TOOLS

THESIS

Presented to the Faculty

Department of Electrical and Computer Engineering

Graduate School of Engineering and Management

Air Force Institute of Technology

Air University

Air Education and Training Command

In Partial Fulfillment of the Requirements for the

Degree of Master of Science in Electrical Engineering

Eugene Johnson, B.S.E.E

1Lt, USAF

December 2004

AFIT/GE/ENG/04-26

TRADE SPACE ANALYSIS OFANTENNA ARRAY ARCHITECTURE USING SYSTEM MODELING TOOLS

Eugene Johnson, BSEE
1Lt, USAF

Approved:

__//signed//_____	_____
Maj Todd B. Hale, Ph.D.	Date
Committee Chairman	
__//signed//_____	_____
Dr Andrew J. Terzuoli	Date
Committee Member	
__//signed//_____	_____
Dr Robert P. Penno	Date
Committee Member	

*Acknowledgement*s

I am deeply grateful to the United States Air Force for giving me the opportunity to engage in a graduate program. My sincerest thanks to my research advisor, the late Major William D. Wood, without whose help and guidance I would not have accomplished this thesis. I would also like to thank my Committee Chairman Maj Todd B. Hale, and other Committee Members Dr. Andrew J. Terzuoli, Dr. Robert P. Penno, for their guidance and support. My thanks also go out to my sponsor and others at the Air Force Research Laboratory, Sensors Division (AFRL/SN) Mr. Kevin V. Sickles, Mr. James P. Theimer, Dr. Dan S. Janning, Dr. Ronald G. Riechers, Mr. David A. Daulton, Mr. Nathan J. Reamer, Mr. Tony K. Quach, and Dr. Charles V. Cerny. I would also like to thank Maj Brian A. Kadrovach at the Air Force Research Laboratory, Space Vehicles Directorate (AFRL/VS), as well as Jerry Marketos and Rulon VanDyke at Eagleware® Corporation.

I would never have attempted or finished this program without the support, love, and patience of my wife and children. Finally, I thank God for granting me faith and wisdom during this academic journey.

Eugene Johnson, III

Table of Contents

Page

List of Figures

Page

List of Tables

List of Symbols

X general expression used in Equations to represent variables……..……..3-9,3-12

β wave number, $2\pi/\lambda$...…….…….…….....2-2

ΔG change in gain……..3-19

δ phase difference between array elements……...……..2-3

ϕ psi, used in geometric representations…….....2-5

λ wave length……..……...……..2-2

ψ psi, variable used to represent $\beta d \cos\theta + \delta$ in array factor Equation.……...2-2

θ theta, used in geometric representations and to represent scan angle….....2-2,3-14,3-18

θ_{bw} actual 3-dB beamwidth……3-20

θ_o desired scan angle……..…3-14

θ_{obw} ideal 3-dB beamwidth……3-18

$(\%chng)_{sx}$ % change in the score…….5-3

$(\%chng)_{opv}$ % change in the output parameter values…….5-3

Abstract

This trade study has two objectives. The first provides a trade space analysis of differing array architectures and associated radio frequency components using system-modeling tools. The second objective develops system modeling tools aiding similar analysis by other users.

These objectives were accomplished by evaluating a selected group of output parameters to include overall system cost, mass, and power consumption, as well as the minimum detectable input level, system spurious free dynamic range, and selected beam spoilage parameters caused by the use of discrete phase shifters. A fixed number of designs were evaluated using simulation.

The evaluation process examined input parameter and design impact on the output parameters and overall best design. The best overall design, by score, performed exceptionally well for minimum detectable input level and beam spoilage parameters, very well for cost and power performance, and poor for total mass and spurious free dynamic range. The best overall design offered a 97% improvement in evaluation score over the lowest scoring design.

The placement of the first stage of low noise amplifiers within the RF component chain, as well as the number of sub-arrays, were among the design parameters found to have the most profound affect on the output results. These results match commonly accepted guidelines in radar design. Selected portions of this study were verified and compared to results from commercially available software, GENESYS® by Eagleware Corporation.

TRADE SPACE ANALYSIS OFANTENNA ARRAY ARCHITECTURE USING SYSTEM MODELING TOOLS

Chapter 1. Introduction

1.1 *Background*

Developing the best antenna array architecture to fit one's application is often a time consuming trial and error process. Engineering judgment alone won't always accomplish the task, as many factors are involved. Some factors to consider are cost, mass (weight), and power consumption. These factors are very important in space-based applications. Other factors to consider are the minimum input level that can be detected by the system, system spurious free dynamic range, and 'beam spoilage' effects on the antenna radiation pattern from the use of discrete phase shifters.

The considerations discussed above are all addressed in this trade study and the accompanying system modeling tools allow users to tailor them to fit their design considerations. The above mentioned factors were evaluated as output parameters. Each of these output parameters were related directly or indirectly to a set of input parameters that defined each one of 2304 specific designs. Each design was scored based on the corresponding output results and ranked accordingly.

Specific near term applications of this thesis work are toward space based autonomous panel type large-scale reconfigurable arrays being developed by the Air

Force. Several Air Force Research Laboratory (AFRL) directorates and divisions have offered inputs, advice, and/or have expressed interest in the results to include the RF sensor technology division (AFRL/SNR), Electromagnetics technology division (AFRL/SNH) and the Aerospace components and subsystems technology division (AFRL/SND) of the Sensors Directorate, as well as the Space Vehicles Directorate (AFRL/VS).

1.2 *Problem Statement*

The overall objective of this research is to provide trade space analysis of differing antenna array architectures using system-modeling tools. The objective is accomplished by investigating both beam spoilage affects of the associated antenna array radiation patterns and Radio Frequency (RF) system component trade-offs affects on various output parameters. The RF component trade-offs include choice of individual components and the components placement/order within the RF component chain.

A secondary objective is to develop an accompanying system modeling tool to allow other users to tailor fit their design considerations when performing analysis on a system of their own specifications.

Software analysis tools are developed whenever practical and commercially available software was used to verify results. This research involves analytical studies only, no hardware experiments were developed.

1.3 *Assumptions*

A complete list of assumptions is listed in section 3.3.2. General basic assumptions used in this trade study were:

1. The only assumed noise present in the system is thermal, or Johnson, noise.
2. All components were assumed to have impedance matching. Also all cabling and connectors were assumed lossless, and therefore not taken into account in the course of this project to include any cost, mass, and power calculations.
3. A constant instantaneous bandwidth was assumed at all points in the receive chain.
4. All components were assumed to be operating in their respective linear region.
5. A cosine radiation pattern was assumed for each array element with uniform amplitude weighting.
6. Component size was not addressed but mass and power considerations were.
7. No grating lobe affects assumed present due to choice of ½ wavelength inter-element spacing and $\pm 60^{\circ}$ area of coverage for the array.

1.4 *Scope*

The scope of this research was limited to analyzing specific tradeoffs between certain vital design parameters. The number of elements per sub-array is one parameter. Another parameter is the first stage of low noise amplifiers' placement within the RF chain. An additional design parameter is the specific RF components with their

associated parameters such as gain, noise figure, third-order intercept point, cost, mass, and power consumption.

Certain parameters are assumed fixed throughout this study. Fixed parameters include the number of elements in the antenna array, antenna element spacing, antenna pattern approximation, uniform element amplitude weighting, single beam formation, frequency of received signal, signal bandwidth, minimum signal-to-noise ratio (SNR) needed above the noise floor for detection, intermediate frequencies (IF), type of detector used, and operating temperatures of components.

Output parameters are evaluated either directly or indirectly from other parameters. Some of these output parameters are minimum detectable signal, system spurious free dynamic range, and beam spoilage effects due to discrete phase shifter quantization. Additional output parameters include total DC power consumption of system components, total cost of system components, and total weight of system components.

1.5 *Methodology*

The overall objectives of this trade study are accomplished by evaluating the output parameters of particular designs, based on the input and fixed parameters, using specific algorithms/code. A fixed number of designs are evaluated with each design defined by its particular input parameters. The output parameters of each design are calculated either directly or indirectly from other parameters.

Most of the input parameters are based on the RF components' parameters such as gain, noise figure, third-order intercept point, cost, mass, and power consumption. Other

input parameters include the number of discrete phase shifter's bits, the number of analog-to-digital converter bits, the antenna array architecture's number of elements per sub-array, the first stage of the low noise amplifiers' placement, and other fixed parameters that will be discussed later in this document.

The output parameters DC power consumption, cost, and mass can simply be determined by adding up the specifications of each component for a particular design. The minimum detectable signal and spurious free dynamic range are calculated indirectly from other intermediate parameters such as system gain, noise figure, and third-order intercept point. These intermediate parameters are calculated from general cascade equations using Matlab®. The cascade equations used are derived from standard academic texts. Beam spoilage parameters are evaluated from the phase shifter quantization effects on the array radiation patterns, such as angle deflection of the array pattern main beam from the ideal scan or steer angle, change in gain of main beam from the ideal radiation pattern, and change in 3-dB beamwidth from the ideal radiation pattern. These beam spoilage effects can be modeled in Matlab®.

Each output parameter is assigned a 'goodness' value from 1 to 10 if the parameter met specifications or a 0 if it did not. For this research, all output parameters are weighted the same, meaning they are all of equal importance with respect to each other. At a later time, if one parameter is deemed more important than another, the scores of each output parameter can be assigned a percentage value to weight it amongst the other output parameters when determining the overall score for each design. The total score for each design was the sum of all the scores for each output parameter for that

particular design. The overall best design had the highest overall score, and the rest were ranked accordingly.

Results from the Matlab® code developed during the course of this study were independently verified with commercially available software to ensure the foundation of this study was accurate.

1.6 *Overview of Document*

This document is broken up into the following chapters that each details a specific study area.

The first chapter is the introduction to the document. Chapter one puts forth the problem, research goals, the study's scope, and methodology overview.

Chapter two is the literature review and provides background information details related to the problem area. Details include background material on antenna arrays, digital beamforming, and a review of RF components and terminology used throughout the study.

The third chapter details the methodology and problem solving approach taken throughout this study. Specifics of chapter three include defining the input, intermediate, and output parameters chosen to be evaluated in this study, and how these parameters relate. Also covered in chapter three are the general equations used throughout this study and implemented in Matlab®. The design evaluation process is discussed in chapter three as well, along with the verification process of results.

Chapter four details the analysis and results. Discussed in chapter four are the analysis trends that were examined, with Matlab® evaluation results presented, as well as the verification of results using commercially available software.

The final chapter of the thesis details the research conclusions and recommendation for future work. Several appendices are contained in this document to include a list of components with specifications in appendix A, the development of noise figure and third order intercept equations for components in parallel in appendix B, and the Matlab® code used in this study in appendix C.

Chapter 2. Literature Review

This literature review provides background material on antenna arrays and digital beam forming techniques currently used in many phased array antenna systems. Also covered is a general review of RF components.

This review begins by first discussing the development of antenna arrays, the characteristics of a standard antenna array, and how a beam (or radiation pattern) is formed and steered. Next, the process of digital beam forming is reviewed and how that process is a useful alternative to analog beam steering. Lastly, the RF components used in this trade study are reviewed as well as some important parameters and definitions.

The material covered in this review is current within the past 15 years, with emphasis on the most recent subject matter because of technological advances in the field of study. This review concentrates on articles/journals that provide general background information on the subject matter. Specific applications are not discussed unless they pertain directly to the thesis topic. Standard academic texts are also referenced as necessary, particularly in review of RF components.

2.1 *Antenna Arrays*

This review begins with the development of antenna arrays, the characteristics of a standard antenna array, and how a beam (or radiation pattern) is formed and steered.

Many single element antennas provide a wide radiation pattern, but low gain or directivity. Many applications require a high gain/directivity antenna, for which the antenna dimensions are required to be increased. One way to increase an antenna's

dimensions is to form a configuration of multiple radiating elements, called an array (Balanis, 1997:249).

A simple and convenient array uses identical elements, with equal amplitude, equal inter-element spacing, and equal inter-element phase difference. Vector addition of the fields radiated by the individual elements, assuming the current in each element is the same as that of the isolated element, determines the array's total field. Balanis lists five controls used to shape the antenna pattern. These controls are:

1. The overall array's geometrical configuration (linear, circular, rectangular, spherical, etc.)
2. The relative displacement between the elements
3. The individual elements' excitation amplitude
4. The individual elements' excitation phase
5. The individual elements' relative pattern

Each of these factors contributes to the array's overall radiation pattern (Balanis, 1997:249).

A single line of elements forms a simple and practical array. To determine the array's total field, a single element positioned at the origin is multiplied by the array factor (Balanis, 1997:250). The Array Factor (AF) is defined as

$$AF = \sum_{n=1}^{N} e^{j(n-1)\psi} = e^{j[(N-1)/2]\psi}\left[\frac{\sin\left(\frac{N\psi}{2}\right)}{\sin\left(\frac{\psi}{2}\right)}\right] \qquad (2\text{-}1)$$

where N is the number of array elements, Ψ is equal to $\beta d \cos\theta + \delta$, β is equal to $2\pi/\lambda$, λ is the wavelength, d is the inter-element spacing, θ is the geometric angle from the z-axis to the direction of radiation assuming the array is oriented parallel to the z-axis, and δ is the phase difference between elements. When the array center is the reference point, the AF becomes

$$AF = \left[\frac{\sin\left(\frac{N\psi}{2}\right)}{\sin\left(\frac{\psi}{2}\right)} \right] \tag{2-2}$$

The normalized array factor is (Balanis, 1997:259)

$$AF_n = \frac{1}{N}\left[\frac{\sin\left(\frac{N\psi}{2}\right)}{\sin\left(\frac{\psi}{2}\right)} \right] \tag{2-3}$$

Figure 2-1 shows the array orientation from which equations (2-1), (2-2), and (2-3) were developed.

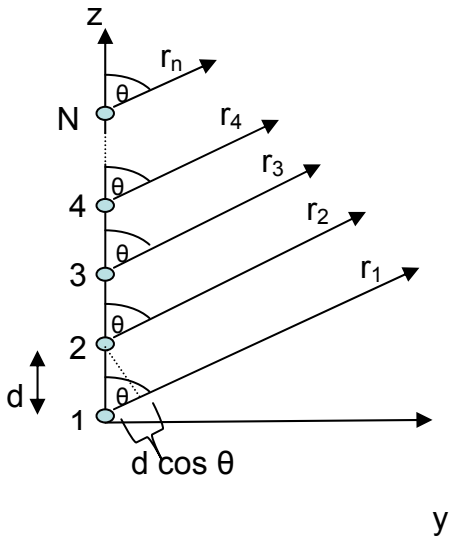

Figure 2-1 Geometry of an N-element array positioned along the z-axis used to develop the array factor, reproduced from (Balanis, 1997:258).

The *AF* maxima occurs when $\Psi = 2n\pi$, where n is an integer. At $n = 0$ the main beam is achieved, and at $n \neq 0$ unwanted minor lobes are present, called grating lobes (Balanis, 1997:262).

Beamforming requires applying complex weights to, and summing the output of, an antenna array's elements to direct the radiation pattern along/toward a specific direction (Litva and Lo, 1996:22; Steyskal, 1996:100-104). Steering the array beam moves the antenna elements' radiation pattern to a desired location. By varying d and/or δ one can control the *AF* and the array total field (Balanis, 1997:250). Some special cases of steering include the broadside and endfire arrays. A maxima for the array factor is achieved at $\Psi = 0$. For a broadside pattern, the goal is to direct the beam toward $\theta = 90^{o}$, so δ is set equal to zero, thus $\Psi = \beta d \cos\theta$. For the endfire pattern δ is set equal to $-\beta d$ to direct toward $\theta = 0^{o}$, or $+\beta d$ to direct toward $\theta = 180^{o}$. To steer the beam to a specific angle θ_i, δ would need to be set equal to $\mp\ \beta d \cos\theta_i$, thus achieving $\Psi = 0$ which is the array factor maxima (Balanis, 1997:262-267).

The linear array case can be extended to planar arrays. For the planar case the AF becomes

$$AF(\theta,\phi) = \left[\frac{\sin\left(\frac{N_x\psi_x}{2}\right)}{N_x \sin\left(\frac{\psi_x}{2}\right)}\right]\left[\frac{\sin\left(\frac{N_y\psi_y}{2}\right)}{N_y \sin\left(\frac{\psi_y}{2}\right)}\right] \qquad (2\text{-}4)$$

where N_x and N_y are the number of array elements in x, and y directions, Ψ_x is equal to $\beta d_x \sin\theta \cos\phi + \delta_x$, Ψ_y is equal to $\beta d_y \sin\theta \sin\phi + \delta_y$, $\delta_{x,y}$ is the phase difference between elements in the x, and y directions, β is equal to $2\pi/\lambda$, λ is the wavelength, d is the inter-

element spacing, θ and ϕ are the geometric angles from the z and x axis to the direction of radiation (Balanis, 1997:311). Figure 2-2 shows the planar array orientation used to derive Equation (2-4).

2.2 *Analog Beamforming*

In an analog system, phase shifters are used to remove the phase delays between array elements, and the outputs from each element are summed to produce one beam. Multiple beams can be produced, but would require NxM phase shifters, where N equals the number of elements in the array and M equals the number of beams to form (Litva and Lo, 1996:24). Figure 2-3 shows an example of analog beamforming. Another method to form multiple beams is using a beamforming matrix, such as the Butler matrix, which uses "multiple hybrid junctions and fixed-phase shifters to produce mutual orthogonal beams" (Litva and Lo, 1996:24). Figure 2-4 shows an example of a Butler matrix.

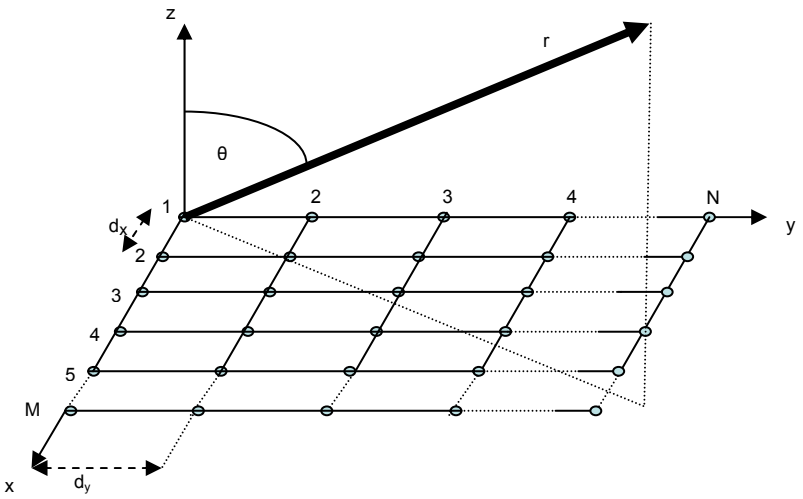

Figure 2-2 Geometry of a planar array used to derive the array factor, reproduced from (Balanis, 1997:310).

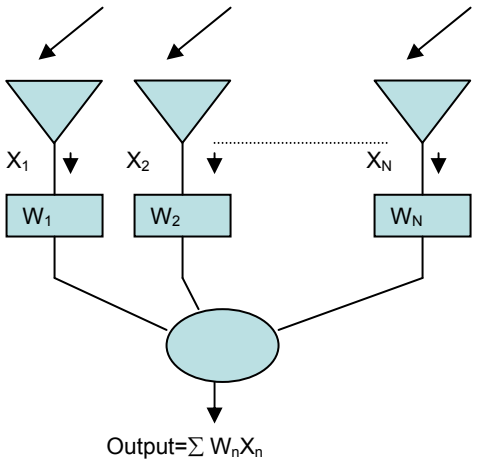

Figure 2-3 Analog Beamforming example, where X_n are the input signals and W_n are the weights applied to the signals, and n = 1,…,N reproduced from (Steyskal, 1996:100).

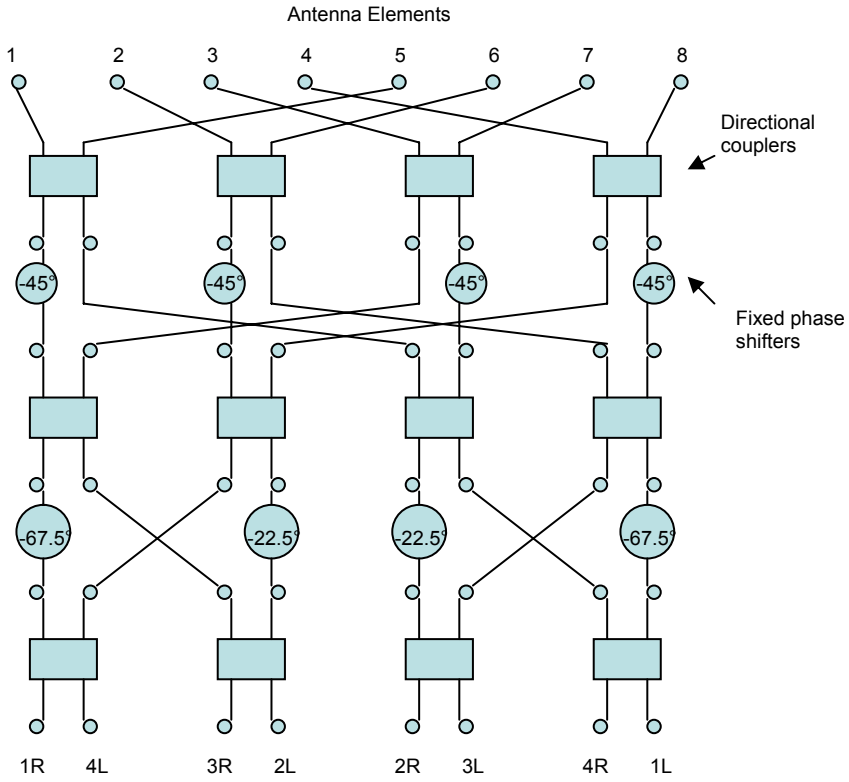

Figure 2-4 Butler Matrix example, a type of beamforming matrix used to produce mutual orthogonal beams, reproduced from (Skolnik, 2001:607).

2.3 *Digital Beamforming*

In contrast to the analog system, digital systems convert the received signal to a lower Intermediate Frequency (IF) for ease of sampling, and digital processing (McCord, 1988:21; Chiba and others, 1997:32; Tanaka and others, 1997:101; Bucciarelli and Picardi, 1988:787; Gupta and Kumar, 2001:191). To steer the beam properly by controlling phase and amplitude, weighting coefficients can be applied to the received signals from each array element (McCord, 1988:1). The actual weights are determined by the beam controller and passed to the beamformer, which combines the weights with the digitized input signals (McCord, 1988:1; Steyskal, 1996:107-108; Steyskal, 1987:114). Figure 2-5 shows an example of digital beamforming, compare to Figure 2-3.

A Digital Beam Forming (DBF) system is especially useful because both the amplitude and phase can be easily changed using a digital processor when forming the desired beam, allowing more control than with a standard array (Chiba and others, 1997:32; Gupta and Kumar, 2001:191).

Another advantage to DBF is the ability to form N beams from N antenna elements. The ability to form multiple beams simultaneously allows covering the desired region of space with those multiple beams, and the beam with the maximum receiving power to be selected (Chiba and others, 1997:32). This advantage of selecting the largest signal also allows the desired incident wave to be automatically tracked (Tanaka and others, 1997:101).

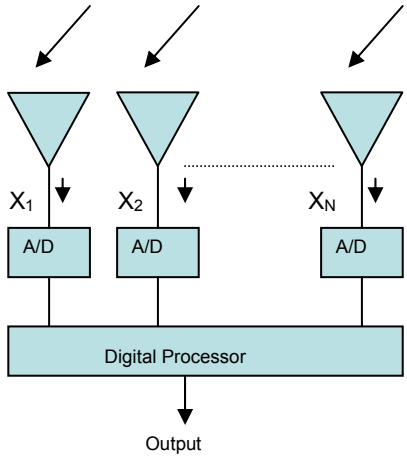

Figure 2-5 Digital beamforming example, where X_n are the input signals, and n = 1,…,N reproduced from (Steyskal, 1996:100).

Another distinct advantage of DBF is the ability to eliminate interference from undesired signals. Applying amplitude and phase weights to an array through the use of DBF gives the ability to sense a desired signal and to attenuate interference (Horton and Abend, 1993:48). DBF allows the beam nulls to be steered to eliminate interference by applying properly determined weights to the input element signals, a type of adaptive weight control and adaptive array signal processing (McCord, 1988:4; Chiba and others 1997:32). It is also possible to generate multiple beams without the received signal levels being degraded using adaptive algorithms and digital processing, and to eliminate unwanted interference (Tanaka and others, 1997:101).

Finally the use of adaptive phased-array antennas provides a cost-effective implementation of large, light weight apertures with high directivity and precise beam shape control (Horton and Abend, 1993:47).

2.4 *Radio Frequency (RF) Components*

RF components associated with antenna arrays when used in a typical radar application are low noise amplifiers, mixers and local oscillators, low-pass and band-pass filters, analog-to-digital converters, and power combiners.

Low noise amplifiers are most critical at the receiver front end where the input signal level is low, and to minimize added input noise. A mixer is used in frequency conversion and ideally allows the sum and difference frequencies of two input signals to be formed. Oscillators provide source signals to be used in the mixing process. Filters are used to pass or reject input signals on the basis of frequency. A low-pass filter will pass signals below a selected cut-off frequency, and reject higher frequencies. A band-pass filter will pass signals within a selected pass-band of frequencies, and reject all others. An analog-to-digital converter converts an input analog signal to a digital signal, which is used later in the digital signal processing stages (Pozar, 2001:19-23). Many other RF components can be used in a radar system, but this research will be limited to the above components.

2.5 *RF Parameters*

The following definitions are of key parameters that were used in this study. As several of these RF parameters can have numerous interpretations, they will be defined now to clarify the context of how they will be used throughout the course of this study. The definitions were taken from standard academic texts and chosen for their context of how they applied to this study.

Gain (G) – Gain is defined to be the ratio of output power to input power (Tsui, 2001:223).

Noise Figure (F) - The noise figure is a measure of the reduction in signal-to-noise ratio between the receiver input and output. The receiver noise figure is defined to be a ratio of the noise out of a practical receiver to the noise out of an ideal receiver (at operating temperature, $T_o = 290K$) or:

$$F = \frac{\left(\frac{S_{in}}{N_{in}}\right)}{\left(\frac{S_{out}}{N_{out}}\right)} \tag{2-5}$$

where S_{in} is the available input signal power, N_{in} is the available input noise power, S_{out} is the available output signal power, and N_{out} is the available output noise power (Skolnik, 2001:34). An ideal receiver would have an F of one, so the range for F is always greater than one.

1-dB compression point - The 1-dB compression point is defined as the input power where the output power deviates 1 dB below the linear gain curve of an ideal case (Pozar, 1990:584). See Figure 2-6.

Third-order intercept point (I) – Third-order intermodulation occurs when two signals f_1 and f_2, of equal amplitude, are input to the receiver and produce two additional products, $2f_1$-f_2 and $2f_2$-f_1 (Skolnik, 2001:737; Tsui, 2001:223-4). See Figure 2-7. The third-order intercept point is defined as the point where the third order intermodulation products and the desired signal are equal in amplitude (Skolnik, 2001:737; Vizmuller, 1995:30-31). Theoretically as the signal level is increased one dB, due to having a linear slope, the third-order product increases by 3 dB, as its slope is three. The third-order

intercept point is typically 10 dB above the 1-dB compression point (Gonzalez, 1984:179). See Figure 2-8.

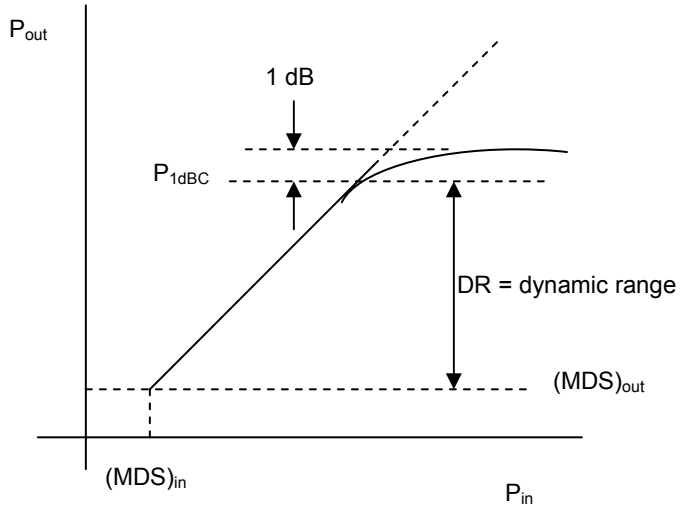

Figure 2-6 1-dB compression point / Dynamic range demonstrated with linear gain curve, reproduced from (Vendelin, 1990:236).

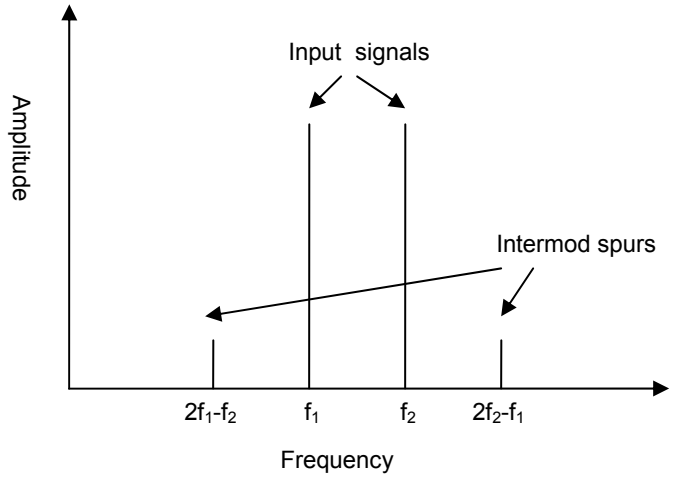

Figure 2-7 Third-order intermodulation products with associated frequency components, plotted frequency vs. amplitude, reproduced from (Tsui, 2001:224).

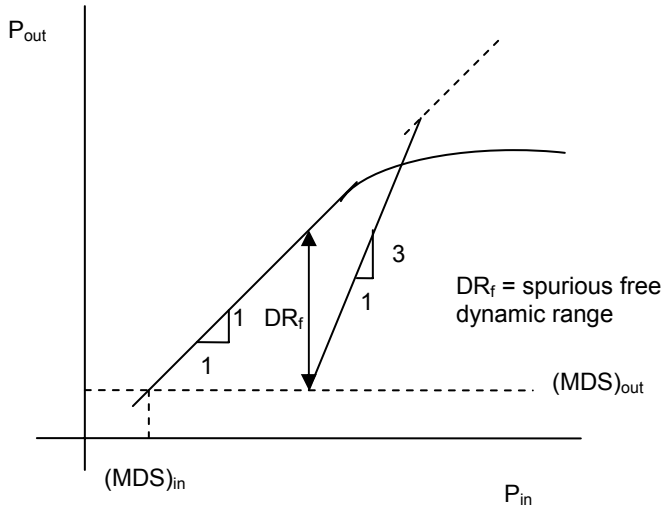

Figure 2-8 Third-order intercept point / Spurious free dynamic range demonstrated with linear gain curve, reproduced from (Vendelin, 1990:236).

Dynamic Range (DR) – The receiver dynamic range is defined to be a ratio of the max input signal power to the min input signal power, without degradation in performance, where the 1-dB compression point typically defines the maximum input signal power, and the minimum input signal is defined by the minimum detectable signal (Skolnik, 2001:737). See Figure 2-6.

Spurious Free Dynamic Range (SFDR) - The receiver spurious free dynamic range is defined to be the ratio of the maximum input signal power that does not generate detectable third-order intermodulation distortion to the minimum detectable signal (Tsui, 2001:28). Or as expressed in dB:

$$\left(SFDR\right)_{rcv} = \frac{2}{3}\left(I - \left(S_o\right)_{\min}\right) \tag{2-6}$$

where I is the third-order intercept point in dB, and $(S_o)_{min}$ is the minimum detectable output signal in dB (Gonzalez, 1984:179). See Figure 2-8. SFDR is less than the DR because of the constraints of limiting intermodulation products and other spurious

responses in the receiver. The SFDR of an analog-to-digital converter, expressed in dB, is defined to be

$$(SFDR)_{A/D} = 10\log_{10}\left(\frac{P_{\max}}{N_b}\right) = 10\log_{10}\frac{\left(\frac{2^{2b}Q^2}{8}\right)}{\left(\frac{Q^2}{12}\right)} = 10\log_{10}\left(\frac{3}{2}2^{2b}\right) = 6b + 1.76, \quad (2\text{-}7)$$

where P_{max} is the maximum power into the A/D, N_b is the quantization noise power which is calculated from the error between the true value of the sine wave and the quantized wave, b is the number of analog-to-digital converter bits, and Q is the voltage per quantization level (Tsui, 2001:165-7).

Minimum detectable signal ($(S)_{min}$) - The minimum detectable input level is defined to be:

$$(S_i)_{\min} = kT_oBF\left(S_o/N_o\right)_{\min} \quad (2\text{-}8)$$

where k is Boltzmann's constant ($1.38\text{x}10^{-23}$ J/K), T_O is operating temperature (290K), B is receiver bandwidth, F is the receiver noise figure, and $(S_O/N_O)_{min}$ is the minimum signal-to-noise ration needed above the noise floor (Pozar, 2001:342). The minimum output detectable signal level is defined to be:

$$(S_o)_{\min} = (S_i)_{\min} G \quad (2\text{-}9)$$

where G is the receiver gain.

2.6 *Chapter Summary*

This literature review has provided background material on antenna arrays and digital beam forming techniques, as well as a general review of RF components. Specific topics included the development of antenna arrays, the characteristics of a standard antenna array, and how a beam (or radiation pattern) is formed and steered. Other topics included a review of the process of digital beam forming, and how that process is a useful alternative to analog beam steering, along with a review of the RF components used in this trade study, as well as some important parameters and definitions.

The topics discussed in this chapter laid the foundation for the trade study that is further detailed later. The equations outlined in this chapter were later implemented in Matlab® and used in the analysis laid out in chapter three. Specific parameters that will be referred to later and corresponding analysis were defined in this chapter. The next chapter details the methodology used throughout this study to implement the necessary analysis to achieve the specified results.

Chapter 3. Methodology

3.1 *General Methodology*

This chapter details the methodology used throughout this study. In this chapter, details of the key input, intermediate, and output parameters are discussed. Also within this chapter, equations are developed that are consequently used in Matlab® and the design evaluation process is outlined. The validation and verification of results is also outlined later in this chapter. The methodology outlined leads directly to the results presented in chapter four.

The objective of this research is to perform a trade space analysis at a system level of differing antenna array architectures and their associated RF components. This objective is accomplished by evaluating a chosen set of output parameters that were calculated either directly from a set of input parameters that define each particular design, or indirectly from some intermediate parameters calculated from the input parameters. The evaluations are performed using algorithms and equations implemented in Matlab®. The exact input, intermediate, and output parameters are discussed further in this chapter, as well as the algorithms and equations implemented. Equations developed in the course of this study were independently verified by commercially available software to ensure their validity.

3.2 *System Level*

At a system level the antenna architecture and RF components are chosen based on real world applications, sponsor input, and interaction with subject matter experts at the Air Force Research Laboratory, Sensors Directorate (AFRL/SN) and the Air Force Institute of Technology, Engineering Department (AFIT/ENG). A system level block diagram is shown in Figure 3-1 and Figure 3-2, these figures show the two placement options for the low noise amplifiers as hardware architecture choices.

The components chosen include antenna array elements, low noise amplifiers, discrete phase shifters, power combiners, mixers, bandpass and lowpass filters, and analog-to-digital converters. Figure 3-1 and Figure 3-2 show the configuration of the components.

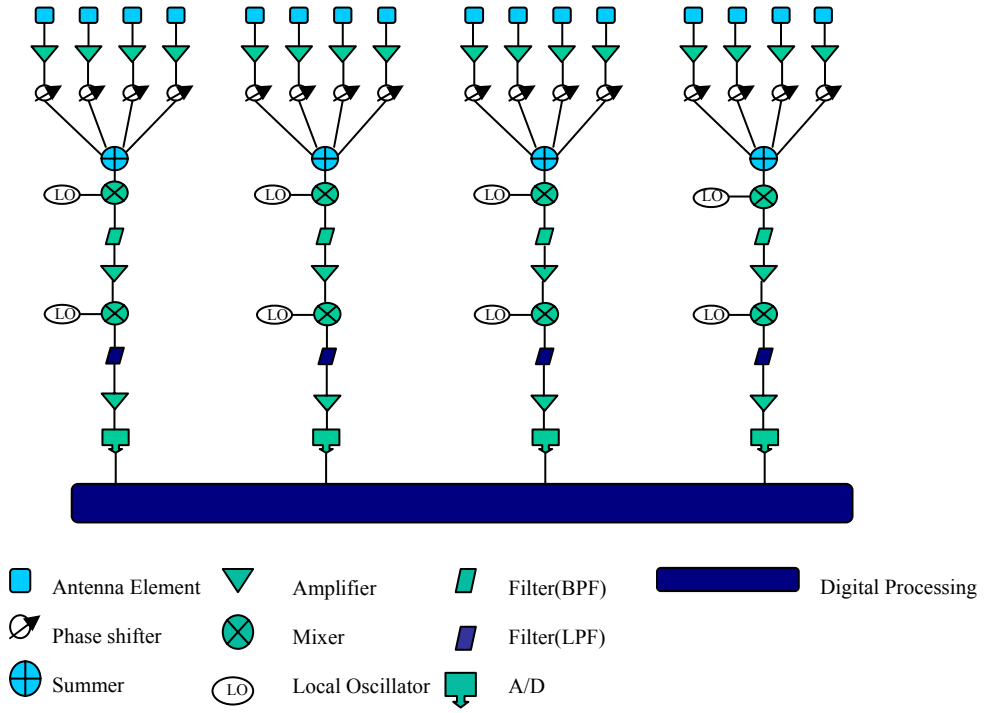

Figure 3-1 System block diagram with low noise amplifiers as the first component in the receive chain

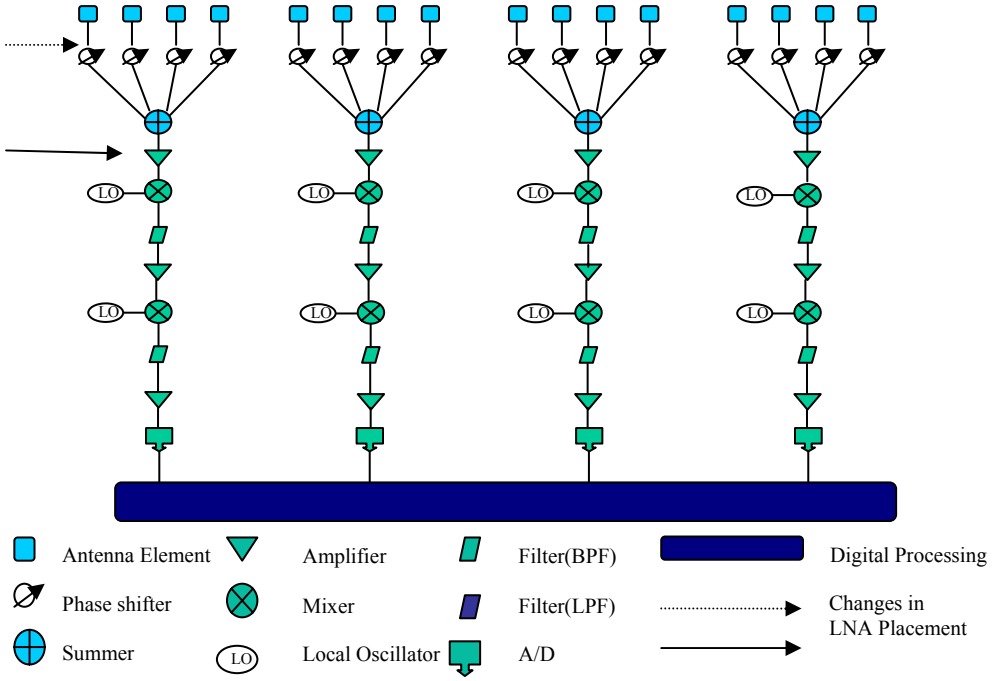

Figure 3-2 System block diagram with low noise amplifiers placed later in the receive chain after sub-arrays/power combiner

One of the hardware architecture configurations chosen to vary is the placement of the first stage of Low Noise Amplifiers (LNA). Figure 3-1 and Figure 3-2 show the two options. The two choices of placement are upfront in the configuration, just after the antenna element and before the other RF components, while the second choice is after the sub-arraying of the elements, just after the power combiner in the configuration. For the choice of placement of the LNAs there are advantages and disadvantages to each type of placement, effecting cost, mass, power consumption, F, $(S_i)_{min}$, and $SFDR$.

The other hardware architecture configuration that is varied is the number of elements per sub-array. The case of four elements per sub-array is shown in Figure 3-1 and Figure 3-2. While holding the number of elements in the array fixed, the ratio of the total number of elements in the array to the number of sub-arrays in the array is varied, thus changing the number of elements per sub-array (M). By varying this ratio a limited

amount of elements could be evaluated, while still preserving a feel of how a larger array would operate. The ratios compared were one, two, four and eight.

The antenna elements were arranged as shown in Figure 3-3. This figure shows the geometry for a uniform array with elements centered along the y-axis, and forms the basis for evaluation throughout this study. The reference element is now chosen to be the center of the array, and this changes the index of the summation in Equation (3-1) when compared to Equation (2-1). This orientation of the array elements was used during the development of the corresponding Matlab® code used for analysis in this study.

The array factor of this particular array configuration is

$$AF = \sum_{n=-[(N-1)/2]}^{[(N-1)/2]} e^{jn\psi} = \left[\frac{\sin\left(\frac{N\psi}{2}\right)}{\sin\left(\frac{\psi}{2}\right)} \right] \qquad (3\text{-}1)$$

which can be compared to equation (2-1), but with Ψ equal to $\beta d \sin\theta + \delta$ due to the geometry involved.

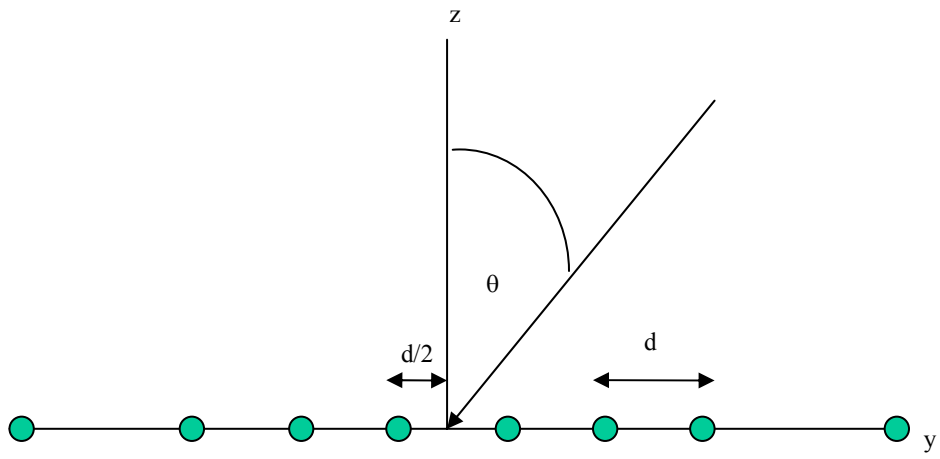

Figure 3-3 Geometry of a uniform array, oriented horizontally, with the reference point the center of the array

3.3 *Input Parameters*

3.3.1 *Variable Parameters*

The hardware architecture parameters of placement of the first stage of low noise amplifiers and the number of elements per sub-array are discussed above in section 3.2. These variable parameters were chosen based on recommendations from the sponsor, as well as subject matter experts in AFRL/SND, and are based on current standard practice and to be aligned with potential future applications.

Other variable parameters are based on the selection of the RF components used in this project. The parameters of gain, noise figure, third-order intercept point, cost, mass, and DC power consumption were all input parameters based on RF component characteristics. Gain, noise figure, third-order intercept point, and their usage throughout this study are defined in section 2.5. Each of these RF component parameter values were found from specification sheets or direct contact with real world manufacturers. A list of the components by type and manufacturer is included in Appendix A. For passive components (such as filters) where only gain or insertion loss is given in dB, the other parameters of noise figure and third-order intercept point could be determined. From the insertion loss, gain could be found as the negative of the insertion loss, noise figure is set equal to the insertion loss, and the third order intercept point was set to be a high value of 100dBm (Tsui, 2001:227).

Additional input parameters are the number of bits of the analog-to-digital converters, the number of bits of the discrete phase shifters, and the scan or steer angles for the array and sub-array which were varied from $\pm 60^{\circ}$.

These input parameters are chosen because they define each particular component as it relates to the determination of the output parameters and any intermediate parameters. As a whole, the input parameters of all the components in each design define that particular design, and gave a reference of that particular design when relating to other designs in the study. Also trends in the output parameters can be related back to a particular input parameter or set of input parameters.

3.3.2 *Fixed Parameters and Assumption*

General assumptions about this trade study are discussed in section 1.3 above. Additional fixed parameters are as follows:

1. The number of elements in the array (N) – The number of elements in the array is fixed at 32 elements. This choice of N allows for easier hand calculations, computations, and structural layout of components in supporting software applications.
2. Antenna inter-element spacing (d) – The inter-element spacing is set at ½ wavelength ($\lambda/2$) for the purposes of this study. This spacing interval is the standard spacing to minimize the effects of grating lobes. Using ½ wavelength spacing and area of coverage of $\pm 60^{\circ}$ guarantees no grating lobes are present in the radiation pattern.
3. Approximation of element pattern – A cosine approximation for the element pattern is used, i.e. $\cos(\theta)$, where the relationship of θ was shown in Figure 3-3. This choice is a good approximation of the actual pattern, and is a standard for use in testing antenna array performance.

4. Element illumination – Uniform amplitude illumination for all elements is assumed throughout this study. Although other types of illumination can be used, this type will ease the calculation/computations within the study.
5. Frequency of received signal (f) – The frequency of the received signal is set at 10 GHz throughout this study. This choice is aligned with probable real world space based applications, such as a large space based reconfigurable array.
6. Instantaneous bandwidth (B) – The instantaneous bandwidth of all components used in this study is chosen to be 200 MHz, and was chosen based the sponsor's recommendation to be aligned with probable future applications, such as spaced based radar applications.
7. Minimum signal-to-noise ratio (SNR) needed – The minimum SNR needed to determine the minimum detectable input level was set at 3dB above the noise floor, this SNR level is the standard of many texts referenced for this study (Vendelin, 1990:235)(Gonzalez, 1984:176).
8. Operating temperatures of components (T_o) – The standard temperature of T_o, 290°K, will be used for all component temperatures, including the antenna temperature (T_a).

These fixed parameters are summarized in Table 3-1.

Table 3-1 Table of parameter values assumed fixed during course of study

Parameter	Value
Number of Array Elements (N)	32
Array Element Spacing (d)	$\lambda/2$
Element Pattern Approximation	Cosine
Element Illumination	Uniform
Frequency of Operation (f)	10 GHz
Instantaneous Bandwidth (B)	200 MHz
Minimum SNR Above the Noise Floor For Detection	3 dB
Operating Temperature of Components (T_o)	290 K

3.4 *Intermediate Parameters*

3.4.1 *Intermediate Parameters Defined*

Several intermediate parameters are calculated from some of the input parameters. These intermediate parameters led to the calculation of many of the output parameters. The three intermediate parameters used in this study are overall system gain, system noise figure, and system third-order intercept point as defined in section 2.5. These three intermediate parameters are found using cascade equations derived from standard textbooks from Gonzalez, Pozar, Skolnik, Tsui, and Vizmuller, and the exact equations are discussed in section 3.4.2 below.

The use of the term ‘overall system’ refers to parameters being found for a complete receive channel of the system as whole, vice for each component separately as was the case for the input parameters. A complete receive channel of the system covers from the first RF component, either the first LNA or the discrete phase shifter depending on hardware architecture chosen, to the front end of the analog-to-digital converter of a particular receive channel, see Figure 3-1 and Figure 3-2 for a system level block

diagram. All receive channels are assumed identical, ignoring any possible random errors, such as phase errors, non-ideal equipment, timing delays, etc.

Overall system gain is directly related to the input parameter gain for each RF component, and leads directly to the output parameter system spurious free dynamic range. Overall system noise figure is directly related to the input parameters of noise figure and gain of the individual components, and in turn leads to the output parameters minimum detectable input level, and spurious free dynamic range. The overall third-order intercept point is found directly from the input parameters gain and third-order intercept point for each component, and also leads to the calculation of output parameter spurious free dynamic range. For the exact equations and how the parameters relate see section 3.4.2 for intermediate parameters and section 3.5.2 for output parameters.

3.4.2 *Design Equations for Intermediate Parameters*

Before performing the design equations for the intermediate parameters the input parameters gain (G), noise figure (F), and third-order intercept point (I), are converted from their initial form of dB into linear form for use in the cascaded intermediate parameter equations as follows:

$$X = 10^{XdB/10} \tag{3-2}$$

where X can be either G, F, or I in dB form in exponent and linear form in result (Tsui, 2001:227) (Vizmuller, 1995:15).

For components in series, standard cascade equations derived from academic texts are used. In the parallel case, at the power combiner after sub-arraying, a more detailed approach has to be taken where the effects of the coherent addition of the signal and

incoherent addition of the noise are investigated for the power combiner. Please see Figure 3-1 and Figure 3-2 for a review of the system level diagram.

For overall system gain the following equation is used:

$$G = \prod_{i=1}^{n} G_i \tag{3-3}$$

where G is overall gain in linear form, G_i is the gain of the ith component, and n is the number of components (Tsui, 2001:226).

To determine the overall system noise figure the following equation sums up the iteration process that is used for the serial components, both before and then after the power combiner:

$$F = F_1 + \sum_{i=2}^{n} \left[\frac{F_i - 1}{\prod_{j=2}^{i} G_{(j-1)}} \right] \tag{3-4}$$

where F is the overall noise figure in linear form, F_i is the noise figure of the ith component, G_i is the gain of the ith component , n is the number of components. This formula is based on the Friis Formula,

$$F = F_1 + \frac{F_2 - 1}{G_1} + \frac{F_3 - 1}{G_1 G_2} + \cdots + \frac{F_n - 1}{G_1 G_2 \cdots G_{n-1}} \tag{3-5}$$

where F is the overall noise figure in linear form, F_n is the noise figure nth component, and G_n is the gain of the nth component (Tsui, 2001:227) (Vizmuller 1995:15) (Skolnik, 2001:731). This proper use of this formula assumes all components have the same bandwidth, for the purposes of this study this assumption is accepted and stated in section 1.3 above. For the parallel case at the power combiner:

$$F_{out} = \frac{F_{in}}{M} \tag{3-6}$$

where F_{out} is the noise figure after the combiner in linear form, F_{in} is the noise figure before the power combiner and M is the number of input ports (number of elements per sub-array). For a complete development of the parallel equation for noise figure see Appendix B.

To determine the overall system third-order intercept point the following equation sums up the iteration process that was used for the serial components, both before and after the power combiner:

$$I = \frac{1}{\sum_{i=1}^{(n-1)} \left[\frac{1}{\left(\prod_{j=i+1}^{n} G_j \right) I_i} \right] + \frac{1}{I_n}} \tag{3-7}$$

where I is the overall third-order intercept point in linear form, I_i is the third-order intercept point of the ith component, G_i is the gain of the ith component, and n is the number of components. This formula was based on the following equation derived from Tsui:

$$I = \frac{1}{\frac{1}{I_n} + \frac{1}{G_n I_{n-1}} + \cdots + \frac{1}{G_3 \cdots G_n I_2} + \frac{1}{G_2 \cdots G_n I_1}} \tag{3-8}$$

where I is the overall third-order intercept point in linear form, I_n is the third-order intercept point of the nth component, and G_n is the gain of the nth component (Tsui 2001:226). And for the parallel case at the power combiner I_{out} becomes:

$$I_{out} = I_{in} M^2 \tag{3-9}$$

where I is the third-order intercept point in linear form, and M is the number of input ports (number of elements per sub-array). For a complete development of the parallel equation for third-order intercept point see Appendix B.

Once the overall system F, I, and G are found using the above equations they are converted back into dB. The following equation was used to convert from linear form to dB:

$$XdB = 10\log(X) \tag{3-10}$$

where X can be either G, F, or I (Tsui, 2001:227).

3.5 *Output Parameters*

3.5.1 *Output Parameters Defined*

In determining output parameters a few factors were considered based upon discussions with the sponsor and subject matter experts at AFIT/ENG and AFRL/SN. One factor is the proposed real world application. When working with space based applications the parameters of cost, mass, and power consumption can be critical. Another factor is what signal levels could the system detect, and how does the use of discrete phase shifters affect the accuracy of detection based on beam pointing accuracy and other beam spoilage effects. Also under consideration from an RF component standpoint is the system spurious free dynamic range. With those factors under consideration the output parameters chosen to be evaluated in this trade study are:

1. Total cost for the system ($)

2. Total mass/weight for the system (g)

3. Total power consumption for the system (W)

4. Minimum detectable input level ($(Si)_{min}$) for the system (dBm)

5. System spurious free dynamic range (SFDR) (dB)

6. Beam spoilage effects due to phase shifter quantization, such as change in beam pointing angle, change in gain, and change in 3dB beamwidth

The terms "minimum detectable input level" and "spurious free dynamic range" and their usage within this trade study are defined in section 2.5. The six output parameters are found using algorithms and equations developed in Matlab® with the aid of standard textbooks cited below.

For cost, mass, and power consumption the term 'system' is in reference to the entire 32 element array and all its associated components, including several receive channels as discussed in section 3.4.1. For $(S_i)_{min}$ and *SFDR* the term 'system' refers to a complete receive channel as defined in 3.4.1, as each receive channel is identical.

Total system cost is calculated directly from the input parameter cost for each individual component, and is measured in dollars, shown in equations (3-11) and (3-14) in section 3.5.2. Total system mass is also calculated directly from an input parameter, mass of each individual component, and is measured in grams, see equations (3-11) and (3-14). Total system power consumption is directly related to the input parameter power consumption for each component, and is measured in watts, as shown in equations (3-11) and (3-14). Total cost, mass, and power are also affected by several hardware architecture input parameters such as the numbers of elements per sub-array, as the number of elements per sub-array determines the number of receive channels and in turn

the number of each type of component needed. Another important hardware architecture parameter is the location of the first stage of low noise amplifiers, either before or after sub-arraying, thus affecting the total number of LNAs. As the number of elements per sub-array increased, the number of receive channels decreased and thus the number components decreased. See Figure 3-1 and Figure 3-2 for examples of the hardware architecture.

$(S_i)_{min}$ is related to several fixed input parameters and is dependent on the intermediate parameter system *F*, which is in turn related to the input parameter *F* for each component and is discussed in sections 3.4.1 and 3.4.2, and is measured in dBm. Minimum detectable input level could be related back to the incident wave front received by the array.

SFDR for the receive chain is not measured directly but is dependent on the intermediate parameters system *I* and *G*, as well as the output parameter $(S_i)_{min}$. The *SFDR* for the analog-to-digital converter is calculated directly from the input parameter number of A/D bits. System *SFDR* is limited by the lower of the receiver spurious free dynamic range and the A/D spurious free dynamic range, and is stated in dB.

The beam spoilage parameters are calculated by comparing the array patterns of the ideal scanning case, where it is assumed any scan angle is realizable, and the case where discrete phase shifters control the scan angles that can be achieved. The total phase at array element *n* when a scan/steer is applied is

$$\text{total phase term of n}^{\text{th}}\text{ element} = e^{j\beta nd(\sin\theta - \sin\theta_o)} \qquad (3\text{-}11)$$

where n is the element number, β is equal to $2\pi/\lambda$, d is the inter-element spacing, λ is the wavelength, θ is the angle describing scannable space, θ_o is the desired scan angle. The applied phase excitation term of the nth element is

$$\text{applied phase term of } n^{\text{th}} \text{ element} = e^{-j\beta nd\sin\theta_o} \tag{3-12}$$

Once a desired scan/steer angle (θ_o) was chosen, the applied phase at each particular element can be calculated by substituting in for θ_o in the above equation, implemented in Matlab®, for each element. To model the phase shifter correctly the ideal phase values are matched to the closest available phase states of the phase shifter, again implemented in Matlab®. These discrete values of the phase shifter are used to model the sub-array pattern of the non-ideal case. The array pattern is found from pattern multiplication of the element and sub-array patterns as well as other input and fixed parameters related to the antenna elements, such as number of array elements, number of sub-array elements, frequency, element spacing, array and sub-array scan angles, and number of phase shifter bits.

Output parameters, once found, are stored in a matrix, with the output parameters in columns and rows based on the number of designs to be evaluated. For exact equations and how the parameters relate, see section 3.4.2 for intermediate parameters, and section 3.5.2 for output parameters.

3.5.2 *Design Equations for Output Parameters*

For total system cost, mass, and power, the following two equations were used with the choice of equations depending on the where the first stage of LNAs was located. Cost, mass, and power can be calculated using the same equations, as all are found from summing up the contributions of each individual component used in the study for that

particular parameter. If the first stage of LNAs was located before the sub-arraying then the following equation is implemented:

$$X = (NX_1) + (NX_2) + \left(\frac{N}{M}\right)X_{sum} + \left(\frac{N}{M}\right)X_3 + \cdots + \left(\frac{N}{M}\right)X_9 \qquad (3\text{-}13)$$

where X is the overall cost, mass, or power of the system, X_1 is the cost, mass, or power of each first stage LNA, X_2 is the cost, mass, or power of each phase shifter, X_{sum} is the cost, mass, or power of each power combiner, $X_{\#3\text{-}9}$ is the cost of each remaining component after the power combiner (sub-arraying), N is the total number of elements in the array, and M is the number of input ports of the power combiner (elements per sub-array). If the first stage of LNAs are located after the sub-arraying then the following equation was used:

$$X = (NX_2) + \left(\frac{N}{M}\right)X_{sum} + \left(\frac{N}{M}\right)X_1 + \left(\frac{N}{M}\right)X_3 + \cdots + \left(\frac{N}{M}\right)X_9 \qquad (3\text{-}14)$$

For minimum detectable input level the following equation is used, as stated in Equation (2-8):

$$(S_i)_{\min} = kT_oBF\left(S_o/N_o\right)_{\min} \qquad (3\text{-}15)$$

where k is Boltzman's constant $1.38\text{x}10^{-23}$ J/K, T_o is equal to 290K, B is the bandwidth (fixed input parameter), F is the system noise figure (an intermediate parameter), and $(S_o/N_o)_{min}$ is the minimum signal-to-noise ratio needed above the noise floor (fixed input parameter) for input level detection (Pozar, 2001:342). $(S_i)_{min}$ can be related back to the incident field on the array by the following equations:

$$W_i = \frac{P_t}{A_{em}} = \frac{P_t}{\left(\frac{\lambda^2}{4\pi}\right)D_o} \tag{3-16}$$

where W_i is the power density of the incident field in watts/m^2, P_t is the power delivered to the load in watts, A_{em} is the maximum effective aperture area of the antenna element in m^2, λ is the wavelength of the signal in m, and D_o is the directivity of the antenna element (Balanis, 1997:81,86). For this project the minimum incident field was found to correspond to the minimum detectable input level, and P_t is equal to $(S_i)_{min}$, and the directivity at the furthest point in the coverage area ($\pm 60^\circ$) was needed. The expression becomes:

$$(W_i)_{\min} = \frac{(S_i)_{\min}}{\left(\frac{\lambda^2}{4\pi}D\right)} = \frac{(S_i)_{\min}}{\left(\frac{0.03m^2}{4\pi}\left(4\cos\left(60^\circ\right)\right)\right)} = \frac{(S_i)_{\min}}{1.4323\left(10^{-4}\right)} \tag{3-17}$$

where $(W_i)_{min}$ is the minimum detectable incident field power density in watts/m^2, $(S_i)_{min}$ is the minimum detectable input level in watts, λ is the wavelength of the signal in meters, D is the directivity of an element oriented horizontally and approximated with a cosine element pattern, and $\theta = 60^\circ$ being the maximum angle of coverage for this approximation (Balanis, 1997:39,46).

When finding system spurious free dynamic range, the following equations are used to determine the *SFDR* of the receiver and the *SFDR* of the analog-to-digital converter. The overall system spurious free dynamic range was the lesser of the two as discussed in section 3.5.1 above. For spurious free dynamic range of the receiver in dB,

$$(SFDR)_{rcv} = \tfrac{2}{3}\left(I - G - (S_i)_{\min}\right), \tag{3-18}$$

where $(SFDR)_{rcv}$ is the spurious free dynamic range of the receiver, I is the third-order intercept point, G is the overall system gain, and $(S_i)_{min}$ is the minimum detectable input level all given in dB (Gonzalez, 1984:179)(Pozar, 2001:342)(Vendelin, 1990:235). The spurious free dynamic range of the analog-to-digital converter in dB is given by

$$\left(SFDR\right)_{A/D} = 6b + 1.76, \tag{3-19}$$

where $(SFDR)_{A/D}$ is the spurious free dynamic range of the analog-to-digital converter, b is the number of bits of the analog-to-converter (Tsui, 2001:167).

The beam spoilage parameters are found from the array radiation pattern as discussed in section 3.5.1 above. Figure 3-4 shows the relationships used in developing the beam spoilage parameters, details are discussed below. Figure 3-4 is a sample plot taken from the Matlab® code used during the course of this study. The antenna array evaluation part of this code makes use of original code developed by Mr. David Curtis of AFRL/SNHA (Curtis, 2002).

The beam pointing angle is found from the peak value of the array radiation pattern of both the ideal scan case and the discrete phase shifter affected case (actual). A change in beam pointing error, how far off the actual scan angle is from the desired scan angle, is found and then evaluated as a ratio relative to the ideal 3-dB bandwidth. The equation implemented is as follows:

$$\mathrm{R}_{\theta} = \frac{\left|\theta - \theta_o\right|}{\theta_{obw}} \tag{3-20}$$

where R_θ is the angle ratio, θ is the actual scan angle, θ_o is the desired ideal scan angle, and θ_{obw} is the ideal 3-dB beamwidth. Figure 3-4 shows θ, θ_o, θ_{obw} in relation to the array power pattern.

The change in gain of the array patterns, between the ideal and the actual case, was found from the differences of the peak values of the two array radiation patterns and measured in dB relative to the gain of the ideal case, where any scan angle is achievable. The equation implemented was:

$$\Delta G = \left(G_i - G\right) \tag{3-21}$$

where ΔG is the change in gain, G_i is the gain for the ideal scan case, G is the actual gain when using discrete phase shifters. Figure 3-4 shows the relationship of ideal gain and actual gain to the array power pattern.

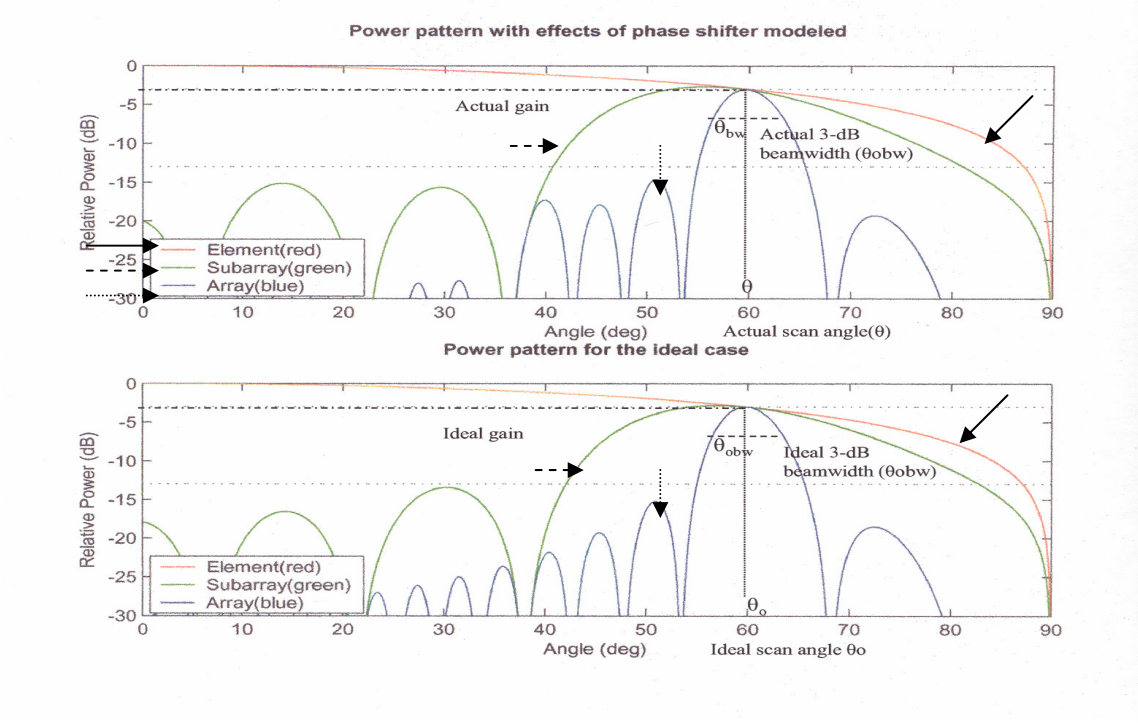

Figure 3-4 Relationship used in developing the beam spoilage parameters, shown using plot of power pattern generated with Matlab®

Change in 3-dB beamwidth is found from a comparison of the 3-dB beamwidths of the two array patterns, and then evaluated as a ratio relative to the ideal 3-dB beamwidth. The equation implemented was:

$$R_{bw} = \frac{\left| (\theta_{\text{bw}}) - (\theta_{\text{obw}}) \right|}{\theta_{\text{bw}}} \tag{3-22}$$

where R_{bw} is the beamwidth ratio, θ_{bw} is the actual 3-dB beamwidth, θ_{obw} is the ideal 3-dB beamwidth. Figure 3-4 shows θ_{bw}, θ_{obw} in relation to the array power pattern.

Acceptable values for all the output parameters are discussed in section 3.6.

3.6 *Design Evaluation*

The total number of different designs that are evaluated depends on the number of choices of each type of hardware architecture parameter, and also the number of choices for each type of component. The total number of designs evaluated is 2304 (N_D), N_D is the total number of possible combinations of RF component and hardware architecture choices. Table 3-2 lists the components or hardware architecture and the number of choices associated with it.

Table 3-2 Table of components / hardware architecture choices

Component or Hardware Architecture	Number of Choices
Elements per sub-array	4
Placement of 1st stage of LNAs	2
LNAs (1st stage)	2
Phase shifters	3
Power combiners	1
Mixers (1st stage)	1
Bandpass filters	2
LNAs (2nd stage)	2
Mixers (2nd stage)	1
Lowpass filters	2
LNAs (3rd stage)	2
Analog-to-digital converters	3

Output parameters for each design are evaluated using Matlab® and the equations listed in section 3.4.2 and 3.5.2. Once the output parameters are found they were assigned a 'goodness' value from 1 to 10, with independent step size based on the range of acceptable values for each particular parameter. See section 3.6.1 below for details on goodness values. The overall score for each design was found by summing the goodness values for each output parameter. The designs were ranked in ascending order. See section 3.6.2 below for details on design rankings.

3.6.1 *Goodness Values*

As discussed, each output parameter, once found, is assigned a 'goodness' value from 1 to 10. This goodness value was simply a score applied to the output parameter results, so each design could be compared to other designs.

For cost, mass, and power consumption each design is ranked in ascending order based on total cost in dollars, mass in grams, and power in watts, and assigned a goodness value as follows:

1. Designs with the highest total (power, cost, and mass) are given a score of 1.

2. Designs with the lowest total (power, cost, and mass) are given a score of 10.
3. Designs are ranked in ascending order from 1 to N_D.
4. For every increase in rank above 1 the score is decreased by -0.0039, (10-1)/N_D.
5. Designs with a tie in parameter values are given the same equal score, skipping the next available score, and then proceeding with the scoring as normal with the next design.

The algorithm used in the calculations is:

$$(Sx)_{c/m/p} = 10 - \left(r_{c/m/p} - 1\right)\left(\frac{9}{N_D - 1}\right) \tag{3-23}$$

where $(Sx)_{c/m/p}$ is the score of cost/mass/power, $r_{c/m/p}$ is the ranking of the current design based on cost, mass, or power, and N_D is the total number of designs that were evaluated (2304). The (-1) included with rank in equation (3-23) was needed to ensure for the design ranked first the score was a 10, and N_D was correspondingly adjusted to ensure consistency for the design ranked #2304 to achieve a score of 1. Figure 3-5 shows a graphical representation of the relationship between cost, mass, and power parameter values and the corresponding score. For cost/mass/power no design is given a 0 score, as compared to the other output parameters, because a 0 score is considered a failure for the purpose of this study. Designs for cost/mass/power are simply ranked in order and not evaluated vs. as specific range of acceptable values.

For minimum detectable input level a range of acceptable values was chosen based on the variables of equation (3-15). For the calculation of $(S_i)_{min}$, kT_o, B, and $(S_o/N_o)_{min}$ all have fixed values. The only variable is system F (intermediate parameter).

An acceptable range of values for noise figure was chosen to be between 2 to 4 dB, based on recommendations by subject matter experts in AFRL/SND as to what should be achievable in a typical RF system of this type and based on probable follow-on applications. Thus, when substituting into Equation (3-15) the range of possible values for $(S_i)_{min}$ became -86 dBm<$(S_i)_{min}$<-84 dBm. $(S_i)_{min}$ for each design is assigned a goodness value as follows:

1. For $(S_i)_{min}$ a value of -84 dBm and above is considered unacceptable and is given a score of 0.
2. -86 dBm<$(S_i)_{min}$ <-84 dBm is acceptable and is given a variable score based on the algorithm below.
3. For $(S_i)_{min} \leq$ -86 dBm is considered optimum and was given a score of 10.
4. For every 0.2 dB, ((-84)-(-86))/10, increase in $(S_i)_{min}$ above -86 dBm there is a reduction of 1 to the score.

The algorithm used in the calculations was:

$$(Sx)_{Si} = 10 - \left((S_i)_{\min} - \max(S_i)_{\min}\right)\left(\frac{1}{0.2}\right) = 10 - \left((S_i)_{\min} + 86\right)5 \qquad (3\text{-}24)$$

where $(Sx)_{Si}$ is the Score for the $(S_i)_{min}$ parameter, max $(S_i)_{min}$ is the maximum possible value of $(S_i)_{min}$ within the acceptable range of values. Figure 3-6 shows a graphical representation of the relationship between the $(S_i)_{min}$ parameter values and the corresponding score.

For *SFDR* a range of acceptable values were chosen based on the sponsor's requirement of 30 to 50 dB of dynamic range based on the one-dB compression point. This dynamic range requirement came from specifications of what should be achievable

in a similar real world application and aligns itself with probable follow-on applications. The corresponding spurious free dynamic range was found to be 26.67 to 40 dB based on the definitions discussed in section 2.5. *SFDR* for each design is assigned a goodness value as follows:

1. For $SFDR \leq 26.67$ dB is considered unacceptable and is given a score of 0.
2. 26.67 dB<*SFDR*<40 dB is acceptable and is given a variable score based on the algorithm below.
3. For $SFDR \geq 40$ dB was considered optimum and is given as score of 10.
4. For every 1.333 dB, (40-26.67)/10, decrease in *SFDR* below 40 dB there is a reduction of 1 to the score.

The algorithm used in the calculation was:

$$(Sx)_{SFDR} = 10 - (\max SFDR - SFDR)\left(\frac{1}{1.333}\right) = 10 - (40 - SFDR)0.75 \qquad (3\text{-}25)$$

where $(Sx)_{SFDR}$ is the score for the *SFDR* parameter, *max SFDR* is the maximum possible value of *SFDR* within the acceptable range of values. Figure 3-7 shows a graphical representation of the relationship between *SFDR* parameter values and the corresponding score.

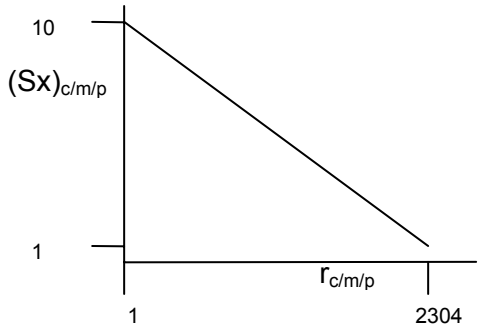

Figure 3-5 Graphical representation of Cost/Mass/Power rankings vs. score for Cost/Mass/Power

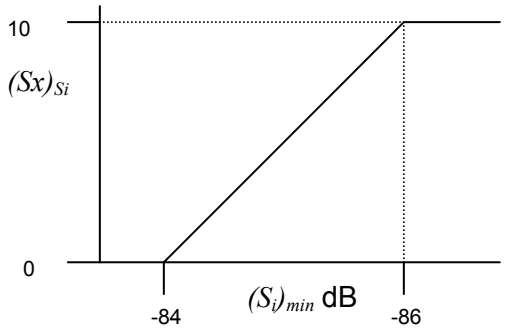

Figure 3-6 Graphical representation of acceptable range of values for $(S_i)_{min}$ vs. score for $(S_i)_{min}$

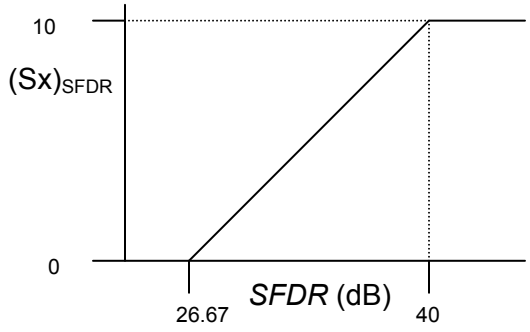

Figure 3-7 Graphical representation of acceptable range of values for *SFDR* vs. score for *SFDR*

For the three beam spoilage parameters each part is given a goodness value score, the scores for each part are summed, then an average score over the three parts is found to give an overall score for beam spoilage. For change in beam pointing accuracy (change in angle) a ratio is found as per section 3.5.2 (Angle Ratio) using equation (3-20). Angle ratio (R_θ) for each design is assigned a goodness value as follows:

1. For any $R_\theta \geq 1$ a loss of coverage in the main beam of the radiation pattern was achieved, due to the discrete angular scan increments (resolution) being greater than or equal to the 3-dB beamwidth of the main beam, and was considered unacceptable and is given a score of 0.
2. $0 < R_\theta < 1$ is acceptable and is given a variable score based on the algorithm below.
3. A R_θ of 0, no change in pointing accuracy, is considered optimum and is given as score of 10.
4. For every 0.1 increase in R_θ above 0 there is a reduction of 1 to the score.

The algorithm used in the calculation is:

$$(Sx)_{R_\theta} = 10 - \left(R_\theta \left(\frac{1}{0.1} \right) \right) = 10 - (10R_\theta) \tag{3-26}$$

where $(Sx)_{R\theta}$ is the score for the angle ratio parameter. Figure 3-8 shows a graphical representation of the relationship between angle ratio parameter values and the corresponding score.

Change in gain, found using Equation (3-21), is assigned a goodness value as follows:

1. For any change in $G \geq 3$dB the main beam of the phase shifter effected pattern is less than ½ the strength of the ideal pattern, and is considered unacceptable and given as score of 0.
2. 0<change in G<3dB is acceptable and is given a variable score based on the algorithm below.
3. No change in G, actual case is equal to ideal case, scored a 10.
4. For every 0.3 increase in change in G above 0 there was a reduction of 1 to the score.

The algorithm used in the calculation was:

$$(Sx)_{\Delta G} = 10 - \Delta G\left(\frac{1}{0.3}\right) = 10 - \Delta G\left(\frac{10}{3}\right) \tag{3-27}$$

where $(Sx)_{\Delta G}$ is the score for the change in gain parameter. Figure 3-9 shows a graphical representation of the relationship between Δgain parameter values and the corresponding score.

For change in 3-dB beamwidth a ratio was found as per section 3.5.2 (Beamwidth Ratio) using equation (3-22). Beamwidth ratio for each design was assigned a goodness value as follows:

1. For any $R_{bw} \geq 0.50$, a 50% widening of the main beam, was considered unacceptable and was given a score of 0, this acceptable ratio level assumes a widening of the beam is unwanted and could be made application dependent.
2. $0 < R_{bw} < 0.5$ was acceptable and was given a variable score based on the algorithm below.

3. A R_{bw} of 0, no widening, was considered optimum and was given as score of 10.

4. For every 0.05 increase in the R_{bw} above 0 there was a reduction of 1 to the score.

The algorithm used in the calculation was:

$$(Sx)_{R_{bw}} = 10 - R_{bw}\left(\frac{1}{0.05}\right) = 10 - (20R_{bw}) \tag{3-28}$$

where $(Sx)_{Rbw}$ is the score for the change in 3-dB beamwidth ratio. Figure 3-10 shows a graphical representation of the relationship between beamwidth ratio parameter values and the corresponding score. The overall score for the beam spoilage parameters is an average of the scores for change in angle ratio, change in gain, and change in 3-dB beamwidth, found as follows:

$$(Sx)_{BS} = \frac{(Sx)_{R_\theta} + (Sx)_{\Delta G} + (Sx)_{R_{bw}}}{3} \tag{3-29}$$

where $(Sx)_{BS}$ is the overall score for beam spoilage.

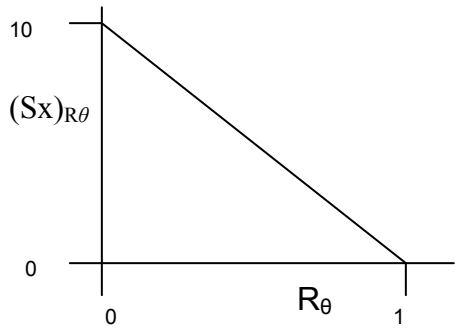

Figure 3-8 Graphical representation of acceptable range of values for R_θ vs. score for R_θ

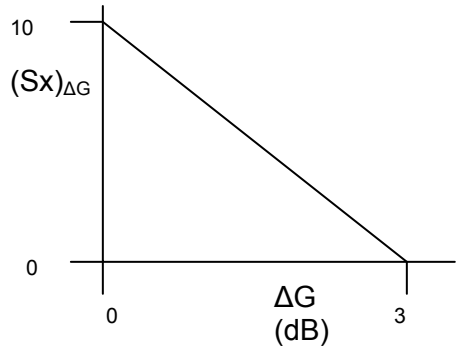

Figure 3-9 Graphical representation of acceptable range of values for ΔG vs. score for ΔG

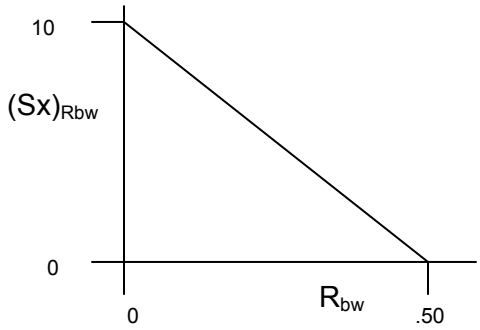

Figure 3-10 Graphical representation of acceptable range of values for R_{bw} vs. score for R_{bw}

3.6.2 *Design Rankings*

All output parameters were given equal weight, meaning they were all considered of equal importance. If for a future study one wished to weigh one parameter higher than another that could be accomplished by applying weighting factors to each of the output parameters scores before combining them for a design score.

The total score for each design was the sum of all the scores for each output parameter of that particular design. The overall best design(s) had the highest overall

score, and the rest were ranked accordingly. Designs were also evaluated based on their performance for each of the output parameters.

3.7 *Validation and Verification*

Results from the Matlab® code developed during the course of this study were independently verified with commercially available software to ensure the validity of the RF related equations used in the corresponding trade study. equations for cost, mass, and power were not verified in this manner. The software used was GENESYS™ RF and Microwave Design Software, developed by Eagleware Corporation®. GENESYS™ software offers a broad range of synthesis, circuit analysis, and electromagnetic simulation products for designing RF and microwave circuits. The particular suite of software used in this study was the system simulation package SPECTRASYS™, which is a spectral domain system simulator developed to aid the user in analyzing and optimizing the RF performance of a chosen architecture consisting of two or more RF elements (Eagleware®, 2004).

In order to properly model the ideal situations laid out in the assumptions in section 1.3 and 3.3.2, the settings for the SPECTRASYS™ schematic had to be adjusted to meet the same assumptions. SPECTRASYS™ accounts for such non-ideal conditions as VSWR between stages, reverse isolation, frequency response, gain compression, frequency rolloff for interfering tones, and broadband noise and image noise that are not taken into account for cascaded equations used in this study. To properly modify the SPECTRASYS™ workspace the VSWR and frequency effects were removed by setting the ripple on the filters used to 0.001 dB, and all ports were set to the same impedance.

The isolation and reverse isolation between elements was set high to 100 dB to reduce bleed through effects. And to remove image noise effects the image rejection was set to 100 dB in all mixers. Also CW signals were used as input sources to limit broadband noise effects. All of these settings were done to reflect, and be consistent with, the ideal conditions assumed in this study. In addition an attenuator was used to replace the phase shifter within the schematics for simulation purposes, as the phase shifter component within SPECTRASYS™ has no input for insertion loss, and this insertion loss was modeled in the Matlab® code used for this study.

The intermediate parameters *G, F,* and *I*, were calculated using SPECTRASYS™ and compared to their corresponding results found in Matlab®. Component input parameters and values were set to match those of design #1 of the Matlab® simulations for the components in series case, and design #577 for the components in parallel case . This choice of input parameters ensured compatibility between the two sets of measurements from SPECTRASYS™ and Matlab®. Both design #1 and design #577, as used in the Matlab® simulations, contained the same component input parameter values, their only difference being the series vs. parallel configuration of their architecture. The exact specifications used in design #1 are detailed in section 5.2. The intermediate parameters *G, F,* and *I* are used directly in the calculations of the output parameters *SFDR* and $(S_i)_{min}$ as detailed in section 3.5, and are a major part of the overall evaluation of this trade study. Using the results obtained for *G, F,* and *I* using SPECTRASYS™ the output parameters *SFDR* and $(S_i)_{min}$ were calculated using equations (3-15) and (3-18) and compared to the results obtained from Matlab®. The results are presented in section 4.2.

Within SPECTRASYS™, cascaded gain is calculated as the desired channel power at the n^{th} stage minus the desired channel power at the first stage, where the desired channel power is the total integrated power in the main channel. The desired channel power ignores intermods, harmonics, and noise, and only considers signals traveling in the forward direction along the schematic path. Cascaded noise figure is calculated as the channel noise power at the n^{th} stage minus the channel noise power at the initial stage minus the cascaded gain at the n^{th} stage, where the channel noise power is the measurement of the integrated noise power in the main channel. The output third order intercept is determined by creating two interfering tones at the input source to create the intermod products within the channel. Cascaded intermod equations are not used in SPECTRASYS™ because they assume the interfering input signals are never attenuated through the cascaded elements (Eagleware®, 2004).

3.8 *Chapter Summary*

This chapter detailed the methodology and problem solving approach used throughout this study. Chapter three provided details of the key input, intermediate, and output parameters. Equations used in Matlab® to achieve the necessary results were presented, the design evaluation process was outlined, and the validation and verification of results was also outlined later in this chapter. The methodology outlined in this chapter led directly to the results presented in the next chapter.

Chapter 4. Model Verification

4.1 *Introduction*

This chapter summarizes the model verification process. The goal of this verification process is to demonstrate the validity of the methodology laid out in chapter three. As stated in section 3.7, results from the Matlab® code developed during the course of this study were independently verified with GENESYS™ RF and Microwave Design Software, developed by Eagleware® Corporation, to ensure the validity of the equations used in this trade study. The SPECTRASYS™ package within GENESYS™ was used to simulate the architecture set forth in section 3.2. SPECTRASYS™ is a spectral domain system simulator developed to aid the user in analyzing and optimizing the RF performance of a chosen architecture consisting of two or more RF elements (Eagleware®, 2004).

4.2 *Matlab® and SPECTRASYS™ Result Comparison*

The intermediate parameters *G, F,* and *I*, were calculated using SPECTRASYS™ and compared to their corresponding results in Matlab®. Component values and specifications were set to match those of design #1 of the Matlab® simulations for the components in series case and design #577 for the components in parallel case. This matching ensured compatibility between the two sets of measurements from SPECTRASYS™ and Matlab®.

A comparison of the values for *G, F,* and *I* using SPECTRASYS™ and Matlab® are shown in Table 4-1, and Table 4-2. Table 4-1 presents the comparisons for the components in series case, and Table 4-2 shows values for the parallel components case. For the parallel case, there is a known inherent difference in gain of approximately 3 dB between the expected result with SPECTRASYS™ and the original result with Matlab®. This -3 dB difference is due to the insertion loss present in the splitters used with SPECTRASYS™. In order for SPECTRASYS™ to treat signals as coherent they must originate from the same source, so an extra splitter must be used after the initial source. The insertion loss of this splitter could not be adjusted during simulations. This difference in gain also affects the results for noise figure, and spurious free dynamic range values of the parallel case. Noise figure is affected because the splitter is now the first component in the receive chain, and is much more noisy than the low noise amplifier that is the first component in the Matlab® analysis. The spurious free dynamic range is directly dependant on the gain as can be seen from equation (3-18).

A percentage of difference in dB between the measurements was found using a modified version of equation (5-2) where $(\%chng)_{OPV}$ is the percentage of change from the Matlab® value, $(V)_{CD}$ is the SPECTRASYS™ value, $(V)_{RD}$ is the Matlab®value, and is shown in Table 4-1 and Table 4-2.

Table 4-1 Comparison of G,F, and I results for SPECTRASYS™ and Matlab® for components in series

Measurement	SPECTRASYS™	Matlab®	Percent Difference in dB
G	72.537 dB	72.50 dB	0.05 %
F	2.456 dB	2.4727 dB	0.68 %
I	15.448 dB	15.6698 dB	1.42 %

Table 4-2 Comparison of G,F, and I results for SPECTRASYS™ and Matlab® for components in parallel

Measurement	SPECTRASYS™	Matlab®	Percent Difference in dB
G	72.362 dB	75.51 dB	4.17 %
F	2.593 dB	2.4727 dB	4.87 %
I	15.448 dB	15.6699 dB	1.42 %

Table 4-3 Comparison of SFDR and $(S_i)_{min}$ results for SPECTRASYS™ and Matlab® for components in series

Measurement	SPECTRASYS™	Matlab®	Percent Difference in dB
SFDR	18.9631 dB	19.1245 dB	0.84 %
$(S_i)_{min}$	-85.5337 dB	-85.5170 dB	0.02 %

Table 4-4 Comparison SFDR and $(S_i)_{min}$ results for SPECTRASYS™ and Matlab® for components in parallel

Measurement	SPECTRASYS™	Matlab®	Percent Difference in dB
SFDR	18.9884 dB	17.1177 dB	10.93 %
$(S_i)_{min}$	-85.3967 dB	-85.5170 dB	0.14 %

Using the results obtained for *G, F,* and *I* using SPECTRASYS™ the output parameters $(S_i)_{min}$ and *SFDR* were calculated using equations (3-15) and (3-18) and compared to the results obtained from Matlab®. The results are shown in Table 4-3, and Table 4-4. The higher percentage difference for *SFDR* for the parallel component case can be explained by the 3 dB difference in *G* between the two measurements as explained above.

4.3 *Chapter Summary*

This chapter provides a summary of the model verification process using commercially available software. As can be seen from the preceding tables the measurements made between SPECTRASYS™ and Matlab® are almost equal, and well within 2 % of each other, except for values resulting from the *G* of the parallel component case as explained above. Thus, overall these results found with

SPECTRASYS™ validate the results found in Matlab® and the equations used throughout this study to generate that Matlab® code. Now that the methodology of chapter three has been verified for accuracy, the results of the study are presented in the next chapter.

Chapter 5. Analysis And Results

5.1 *Introduction*

In this chapter, the results that were generated using the methodology outlined in chapter three are presented and examined. Due to the vast amounts of potential data available from this study, the focus on the analysis was limited to certain trends. The trends were chosen due to their relevance to how the study was set up to examine the choice of input and design parameters' affects on the corresponding output parameters, as well as examine the overall best design by the scoring method established in chapter three. Several subsections within this chapter present the results and analysis for a particular trend. Both the results and analysis for each particular trend are discussed together within the corresponding subsection. The specific trends examined are detailed to greater lengths within this chapter.

Several files/charts were generated to be used in the analysis of the results, these files/charts included scores for each output parameter by design, output parameter values by design, and the overall total score for each design. Other references used in the analysis were a list of components with specifications, a list of design components/hardware architecture choices referencing the design numbers that contained those choices, and a list of designs referencing all their corresponding components, the first chart is included in Appendix A.

Once the output parameters were generated and scored, the results were analyzed for trends. Several trends presented themselves for examination. One of these trends was

the input parameters that had the greatest impact on each output parameter. Another trend looked at was the design(s) including its corresponding RF components and hardware architecture that showed the best performance for a particular output parameter. Also analyzed were the design(s) that had the best overall score and what input parameters/components/architecture that design(s) had.

Results found in Matlab® were verified using the GENESYS™ RF and microwave design software package. A comparison to the Matlab® results are presented in section 4.2.

5.2 *Input Parameter Impact on Each Output Parameter*

The first trend analyzed was which input parameter/component/architecture had the greatest impact on each particular output parameter. This analysis was accomplished by comparing the scores for each output parameter and the actual output parameter values for each design to a reference design. The reference design tied for the best overall score among all designs and was therefore chosen as a convenient reference. Section 5.4 further discusses the top designs and the reference design. Table 5-1 shows the components/architecture parameters of the reference design, design number 2113.

To determine which particular component had the greatest impact on the chosen output parameter, a design with a difference in only one component/architecture choice from the reference design was selected for comparison. This process was repeated by selecting other designs with a single different change in an input choice.

Table 5-1 Reference design specification

Component / Architecture	Choice # / #
Elements per sub-array	8
Phase Shifter	Choice # 3
LNA 1st stage	Choice # 1
BPF	Choice # 1
LNA 2nd stage	Choice # 1
LPF	Choice # 1
LNA 3rd stage	Choice # 1
A/D	Choice # 1
LNA placement	Choice #1

A percentage of change from the reference design score was calculated using the following formula.

$$(\%chng)_{SX} = \frac{((\mathrm{Sx})_{\mathrm{CD}} - (\mathrm{Sx})_{RD})}{(\mathrm{Sx})_{RD}} \times 100 \tag{5-1}$$

where $(\%chng)_{SX}$ is the percentage of change from the reference design score, $(Sx)_{CD}$ is the current design score, $(Sx)_{RD}$ is the reference design score.

Similarly a percentage of change from the reference design output parameter values was calculated using the following formula.

$$(\%chng)_{OPV} = \frac{((\mathrm{V})_{\mathrm{CD}} - (\mathrm{V})_{\mathrm{RD}})}{(\mathrm{V})_{\mathrm{RD}}} \times 100 \tag{5-2}$$

where $(\%chng)_{OPV}$ is the percentage of change from the reference design output parameter value, $(V)_{CD}$ is the current design parameter value, $(V)_{RD}$ is the reference design parameter value.

5.2.1 *Summary of Results for Input Parameter Impact on Each Output Parameter*

Table 5-2 shows a summary of the different component and architecture choices' impact on the output parameter scores, shown as a % change in the score for each

particular output parameter. Table 5-3 shows a summary of the different choices' impact on the output parameter values, again shown as a % change. Table 5-4 shows a summary of the component/architecture choices that had a major impact on the corresponding output parameter. Note Table 5-2 and Table 5-3 do not list the components present in the reference design, see Table 5-1, and scores and values shown were calculated from equations (4-1) and (4-2) as discussed in section 5.2.

Table 5-2 Summary of component and architecture choices' impact in % of change on output parameter ***scores***

		Output Parameters					
		$(S_i)_{min}$	*SFDR*	*Cost*	*Mass*	*Power*	*Beam Spoilage*
Component/ Architecture Choice	LNA placement #2	(-)100%	0%	* 0 to 14.56%	* 0 to 24.37%	* 0 to 34.15%	No Impact
	LNA1 choice #2	(-)100%	0%	6.35%	(-)2.06%	(-)4.86%	
	LNA2 choice #2	0%	0%	0%	0%	0%	
	LNA3 choice #3	0%	0%	1.49%	(-)24.68%	(-)1.62%	
	PS choice #1	(-)24.15%	0%	(-)5.97%	8.23%	(-)5.27%	(-)0.07%
	PS choice #2	(-)24.15%	0%	11.57%	6.17%	0.41%	0%
	1 element/sub-array	No Impact	0%	‡	‡	‡	0.10%
	2 elements/sub-array		0%	‡	‡	‡	0.05%
	4 elements/sub-array		0%	‡	‡	‡	0.04%
	Combiner (1)*	†	†	(-)49.65%	102.84%	(-)58.74%	†
	Combiner (2)*	†	†	(-)42.56%	49.36%	(-)43.75%	†
	Combiner (4)*	†	†	(-)14.56%	(-)49.36%	(-)14.58%	†
	A/D choice #2	No Impact		(-)11.57%	No Impact	(-)0.81%	No Impact
	A/D choice #3			(-)14.19%		(-)2.43%	

Notes: * -(#) for the combiner refers to the number of elements per sub-array; * -the varying amount of change for LNA placement choice #2 for cost, mass, and power is due to the varying effect of the number of elements per sub-array); † -changes referenced in elements/sub-array section of table; ‡ -changes referenced in combiner section of table

Table 5-3 Summary of component and architecture choices' impact in % of change on output parameter ***values***

		Output Parameters					
		$(S_i)_{min}$	*SFDR*	*Cost*	*Mass*	*Power*	*Beam Spoilage*
Component/ Architecture Choice	LNA placement #2	(-)9.10%	(-)48.30%	* 0 to (-)20.35%	* 0 to (-)0.02%	* 0 to (-)60.72%	No Impact
	LNA1 choice #2	(-)9.00%	57.05%	(-)6.26%	0.01%	7.47%	
	LNA2 choice #2	0%	(-)43.09%	0%	0%	0%	
	LNA3 choice #3	0%	58.01%	(-)0.83%	0.29%	1.00%	
	PS choice #1	(-)0.65%	21.19%	6.71%	(-)0.02%	7.78%	° 33.59%/ 237.20/ (-)2.44%
	PS choice #2	(-)0.65%	21.19%	(-)15.20%	(-)0.01%	(-)0.04%	° 0%/0% /0%
	1 element/sub-array	No Impact	55.68%	‡	‡	‡	° (-)100%/ (-)100%/ (-)2.44%
	2 elements/sub-array		37.12%	‡	‡	‡	° (-)63.29/ (-)13.28%/ (-)2.44%
	4 elements/sub-array		18.56%	‡	‡	‡	° (-)33.09/ (-)6.42%/ (-)2.44%
	Combiner (1)*	†	†	95.42%	(-)24.96%	213.90%	†
	Combiner (2)*	†	†	72.84%	(-)21.18%	91.67%	†
	Combiner (4)*	†	†	19.62%	51.79%	30.56%	†
	A/D choice #2	No Impact		13.93%	No Impact	0.53%	No Impact
	A/D choice #3			19.31%		1.42%	

Notes: * -(#) for the combiner refers to the number of elements per sub-array; * -the varying amount of change for LNA placement choice #2 for cost, mass, and power is due to the varying effect of the number of elements per sub-array); † -changes referenced in elements/sub-array section of table; ‡ -changes referenced in combiner section of table; ° -for beam spoilage there were three separate parameters measured, they are listed as beam width ratio/gain/angle ratio.

Table 5-4 Component and architecture choices that had a major impact on each output parameter

	Output Parameter	$(S_i)_{min}$	SFDR	Cost	Mass	Power	Beam Spoilage
Component/Architecture Choice							
LNA Placement		√	√			√	
1st stage of LNAs		√	√				
2nd stage of LNAs			√				
3rd stage of LNAs			√				
# of elements per sub-array				√	√	√	√
Power Combiner					√		
Phase Shifter							√

5.2.2 *Impact on $(S_i)_{min}$*

For $(S_i)_{min}$, all designs with the low noise amplifiers placed after the sub-arrays/power combiners (LNA placement choice #2) failed to meet the $(S_i)_{min}$ acceptable threshold. This failure to meet the acceptable threshold was due to the negative effect on the overall noise figure of the system by placing a noisier component upfront in the receiver chain, and F directly impacts $(S_i)_{min}$, see equation (3-15). This result matches commonly accepted guidelines in radar design.

All designs with the first stage of low noise amplifiers choice number two (LNA1 choice #2) also fail to meet the minimum acceptable values. LNA1 choice #2 has a 133% higher noise figure in dB than choice #1 (a list of components and their specifications is listed in Appendix A), and when used as the first component in the receive chain (LNA placement choice #1) has an even greater negative impact on $(S_i)_{min}$.

The choice of phase shifters used in the system also impacts $(S_i)_{min}$, as this is either the first or second component in the RF chain. A noisier component has a negative effect on overall system noise figure, and increasing system noise figure lowers $(S_i)_{min}$. Phase shifter choice #1 and #2 (PS choice #1 and #2) had an 80% higher noise figure than phase shifter choice three (PS choice #3).

The parameters that had the biggest effect on $(S_i)_{min}$ performance were the placement of the first stage of low noise amplifiers, and the choice of the first stage of low noise amplifiers. This effect was due to the effect those choices had upon the system noise figure (an intermediate parameter), which in turn directly affects $(S_i)_{min}$.

5.2.3 *Impact on SFDR*

Most designs failed this specification, due to the high cascaded gain of the system. By using three stages of low noise amplifiers in the RF chain, the overall system gain was increased dramatically.

Placing the first stage of low noise amplifiers later in the receive chain had a negative impact on *SFDR* performance due to placing the higher gain later in the receive chain, thus impacting the third-order intercept point which in turn affects the spurious free dynamic range, see equations (3-8) and (3-18). Also, this placement increased the system noise figure, lowering $(S_i)_{min}$ (less negative), thus lowering the *SFDR* which is dependent on $(S_i)_{min}$.

The choice of low noise amplifiers (LNA) also had an impact on *SFDR*. LNA2 choice #2 had a negative impact on *SFDR*, due to having a higher gain (53.8%) and noise figure (9.1%) than choice #1. This impact more than offset having a higher third-order intercept point (70%) than choice #1. Increasing *G* and *F* reduces *SFDR*, while increasing *I* increases SFDR see equations (3-15) and (3-18). The choice of the third stage of low noise amplifiers (LNA3) impacted *SFDR* as well. LNA3 choice #2 had a positive impact on *SFDR*, due to having lower *G* (-7.3%) and higher *I* (75%) than choice #1, this offset having a higher *F* (58.8%). LNA1 choice #2 also had a positive effect on

SFDR, due to having lower *G* (-65.4%) and higher *I* (31.0%) than choice #1, this offset having higher *F* (133.33%).

PS choice #1 and #2 had positive impacts as well. Both choices had lower *G* (-80%), and this offset having higher *F* (80%).

The number of elements per sub-array also impacted *SFDR*. Lowering the elements per sub-array increased *SFDR*, due to lowering the overall system gain by having fewer inputs to the power combiner. As the number of elements per sub-array (*M*) increased, the cascaded gain went up by a factor of *M* due to the power combiner. The lowering of the system gain by reducing the number of elements per sub-array more than offset the impact of lowering *I* by M^2 as an effect on *SFDR*.

There were no changes to the *SFDR* scores between designs evaluated when changing a single parameter from the referenced design, due to all the chosen designs failing the specification, but there were changes in values of the output parameter. Table 5-3 shows the % change in the output parameter values for different component choices, and shows the percentage change in the output parameter values for different hardware architecture choices.

The parameters that had the biggest impact on *SFDR* were the choice of the various stages of low noise amplifiers, placement of the first stage of low noise amplifiers, and the number of elements per sub-array. What all these parameters had in common was their effect on the overall system gain. By lowering the gain, especially late in the receive chain as can be shown by the LNA3 choice #2, which only had a -7.3% difference in gain from choice #1 but caused a 58.01% increase in *SFDR*, the *SFDR* increased. By examining the above results, the change in *G* had an even larger impact

than changes in *F* and *I*. All the components with lower *G* improved *SFDR* and all the components with higher *G* reduced *SFDR*, but several of the components with lower *G* also had either higher *F* or lower *I* which would negatively impact *SFDR* but they still caused an increase in *SFDR* due to having lower individual gain. And conversely, several of the components with higher *G* also had either lower *F* or higher *I* which would positively effect *SFDR*, but overall they had a negative effect on *SFDR* due to their higher gain.

5.2.4 *Impact on Cost*

The choice of analog-to-digital converters had a small effect on the overall cost of the system. Designs with analog-to-digital converter choice #2 (A/D choice #2) and A/D choice #3 both had a negative impact on the cost performance of the system due to having higher individual costs than choice #1. A/D choice #2 had a 166.68% higher individual cost than choice #1, and A/D choice #3 had a 231.08% higher cost than choice #1.

LNA3 choice #2 had a small positive effect on overall cost. LNA3 choice #2 had a 29.54% lower individual cost than choice #1. LNA1 choice #2 also had a slight positive impact on overall cost, having a 26.92% lower cost than choice #1. The first stage of low noise amplifiers had a somewhat larger impact on the overall system cost than the third stage due to there being more of the first stage amplifiers when they were placed before the sub-arrays (32 of them), and fewer of the third stage amplifiers (32/*M*) since they were placed later in the receive chain.

The choice of phase shifters had a varying effect on overall cost. PS choice #1 had a negative impact on cost performance, due to having a 17.86% higher individual

cost than choice #3 (the reference). PS choice #2 had a positive impact due to having a 40.48% lower individual cost than choice #3.

Changing the elements per sub-array had several effects on the cost. First different power combiners were needed for each change in the number of elements per sub-array, with none at all for one element per sub-array, and each power combiner had a different individual cost. Also changing the number of elements per sub-array (M) changed the total number of each component needed ($32/M$) after the power combiner/sub-arraying, thus directly impacting the cost of the system. The reference design had eight elements per sub-array. Using one element per sub-array dramatically increased the cost due to having 32 of each of the individual components. When M=2, the cost was still negatively impacted due to having more components than the reference case and the increased cost of using a power combiner. The cost of the combiner when M=2 was 50% cheaper than for the case of M=8, but having fewer elements per sub-array required more individual components. For the case when M=4, the difference from the reference case was lower but still there was an increase in cost. The increase was again due to having more individual components in the system despite having a 43.75% less costly combiner.

The placement of the first stage of LNAs also had an impact on the overall system cost. This impact was due in part to increasing the number of LNAs needed when placing them upfront in the RF chain, before the sub-arrays. A positive effect was created as the number of elements per sub-array increased, as this lowered the overall number of individual components. Placing the first stage of LNAs after the sub-arrays

decreased the number of these components from 32 to 32/*M*, thus decreasing the overall system cost.

Table 5-2 shows the relationship between the choices of components and the impact on the overall system cost scores, and shows the relationship between the choices of hardware architecture to the overall system cost scores. Table 5-3 shows the same relationships but to the overall system cost values.

The largest contributor to cost was the number of elements per sub-array. This effect on cost is due to the affect on the number of individual components needed, as *M* increased the number of components decreased (32/*M*), thus the overall system cost went down.

5.2.5 *Impact on Mass*

The choice of LNAs impacted the overall system mass. The third stage of LNAs had a larger effect than the first stage of LNAs. Even though there were, depending on the placement choice of LNAs, an equal or larger number of the first stage LNAs they were much lighter individually in comparison to the third stage LNAs. LNA1 choice #2 had a small negative affect on the system mass performance, over choice #1. LNA1 choice #2 had 50% more individual mass than choice #2. LNA3 choice #2 also had a negative impact on mass performance, due to having 50% more individual mass than choice #1.

The choice of phase shifters also had an impact on overall mass. Both PS choice #1 and PS choice #2 had a positive impact on mass from choice #3. PS choice #1 had 36.08% less individual mass than choice #3, and PS choice #2 had 27.84% less mass than choice #3.

Changing the elements per sub-array also had several effects on mass. First different power combiners were needed for each change in the number of elements per sub-array, with none at all for one element per sub-array, and each power combiner had a different individual mass specification. Also changing the number of elements per sub-array (M) changed the total number of each component needed ($32/M$) after the sub-arrays, thus directly impacting the mass of the system. The reference design had eight elements per sub-array. The large individual mass of the power combiners for the four elements and eight elements per sub-array case more than offset the decrease in the number of individual components needed, and was the driving factor in the mass of the system. The cases of one and two elements per sub-array had a positive impact on mass, as compared to eight elements per sub-array case, due to the individual weight of the combiner used in the eight elements per sub-array case. The four elements per sub-array case had a negative impact on system mass, due to needing more individual components and only having a moderately lower individual mass of the combiner when compared to the eight elements per sub-array case.

The placement of the first stage of LNAs also had an impact on the overall system mass. This impact was due in part to increasing the number of LNAs when placing them upfront in the RF chain, before the sub-arrays. The effect varied as the number of elements per sub-array increased, as this lowered the overall number of individual components but was somewhat offset by the increase in individual mass of the power combiners for the four and eight elements per sub-array case. LNA placement choices #2 in all cases had either equal mass or lower mass than choice #1. Table 5-2 and Table 5-3

show the impact of the various component and architecture choices on the system mass parameters.

The largest contributor to the overall system mass was the individual mass of the power combiners. As the number of elements per sub-array increased the number of individual components needed decreased by 32/*M*, thus the system mass would decrease. This effect was more than offset by the large individual mass of the power combiners used in sub-arraying, thus the mass actually was higher as the number of elements per sub-array increased, especially in the jump to four elements per sub-array.

5.2.6 *Impact on Power Consumption*

The choice of analog-to-digital converter had a slight impact on the overall system power consumption. A/D choice #2 had small negative impact on the power performance, due to A/D choice #2 having 2.46% higher individual power consumption than choice #1. A/D choice #3 also had higher individual power consumption (6.56%) than choice #1, and a small negative effect on the system power consumption.

The choice of LNAs also impacted the power consumption performance of the system. The first stage of LNAs had more of an impact than the third stage, due to there being more individual components of LNA1 when placed up front in the receive chain and having significantly more individual power consumption than LNA3s in general. LNA1 choice #2 had a negative impact on the system power, due to choice #2 having 10.77% higher individual power consumption than choice #1. Moreover, LNA3 choice #2 had a slight negative impact on system power, due to having 107.14% higher power consumption than choice #1.

PS choice #1 had a negative impact on the system power performance, due to having a 14,566.67% increase in individual power than PS choice #3. PS choice #2 on the other hand had a positive impact on power, due to having a 66.67% decrease in individual power from choice #3.

Changing the elements per sub-array affected the system power by changing the total number of each component needed (32/*M*) after the sub-arrays, thus directly impacting the power performance of the system. As the number of elements per sub-array increased the number of individual components needed decreased and thus the system power consumption decreased.

The placement of the first stage of LNAs also had an impact on the overall system power performance. This impact was due in part to increasing the number of LNAs when placing them upfront in the RF chain, before the sub-arrays. The positive effect was increased as the number of elements per sub-array increased, as this lowered the overall number of individual components. Placing the first stage of LNAs after the sub-arrays decreased the number of these components from 32 to 32/*M*, thus decreasing the overall system power. Table 5-2 and Table 5-3 show the impact of the various component and architecture choices on the system power consumption

The parameter that had the largest impact on system power was the elements per sub-array. This impact was due to the reduction of individual components as *M* increased, thus lowering the overall power consumption. Also having a large impact was the placement of the first stage of low noise amplifiers. By placing the first stage of LNAs later in the receive chain, after the sub-arrays, lowered the number of LNAs needed, thus reducing the overall system power.

5.2.7 *Impact on Beam Spoilage*

The choice of phase shifters had an impact on beam spoilage performance. The number of phase shifter bits directly impacted the actual radiation patterns of the array (discrete phase shifter case), and when compared to the ideal radiation patterns caused changes in the beam spoilage parameters. Phase shifter choice #1 had a negative effect on the beam spoilage outputs, due to PS choice #1 being a 5 bit phase shifter compared to choice #2 and #3 being 6 bit phase shifters. As the number of bits in the phase shifter increased, the closer the actual pattern was to the ideal pattern, thus the beam spoilage parameters improved.

As the number of elements per sub-array varied so did the effects on the beam spoilage parameters. As *M* increased there was a negative effect on the beam spoilage parameters, the beam spoilage scores became lower and the values of the three individual beam spoilage parameters generally increased. Table 5-2 and Table 5-3 show the impact of the various component and architecture choices on the beam spoilage parameters.

The parameters that had the largest effect on beam spoilage were the choice of phase shifter and the number of elements per sub-array. Both of these parameters impacted the radiation patterns of the antenna array for both the ideal case and the actual case using discrete phase shifters, thus causing changes in the beam spoilage parameters that evaluated the differences between them.

5.3 *Design Impact on Each Output Parameter*

The next trend to be analyzed was which particular design or designs, and their corresponding components/architecture choices, achieved the best performance for each

of the output parameters. The analysis was accomplished by determining the top score and parameter value for each output parameter, and then locating which designs had that corresponding score/value. Then these designs were evaluated to determine which components/architectures were selected for each design using a reference file comparing designs to component/architecture choices. From this analysis, key components that caused the particular designs to achieve success for an output parameter were determined.

Components/architecture choices that were shared amongst all of the top designs were deemed key choices that could not be varied without changing the overall performance of the designs. If a particular component/architecture choice changed amongst the top designs then it had a negligible effect on the performance for that particular output parameter being evaluated, and was not considered a key component.

5.3.1 *Summary of Results for Design Impact on Each Output Parameter*

Table 5-5 shows the key components of the top performing designs for the output parameters $(S_i)_{min}$, *SFDR,* Cost, Mass, Power, and Beam Spoilage. Key components for each particular output parameter performance are detailed in the sub-sections that follow.

Table 5-5 Key components of top performing designs by output parameter

		Components						
		Elements/ sub-array	PS choice	LNA1 choice	LNA2 choice	LNA3 choice	LNA placement choice	A/D choice
Output Parameters	$(S_i)_{min}$	N/A	#3	#1	#2	#1	#1	N/A
	SFDR	1	N/A	#2	#1	#2	#1	N/A
	Cost	8	#2	#2	N/A	#2	#2	#1
	Mass	1	#1	#1	N/A	#1	N/A	N/A
	Power	8	#2	#1	N/A	#1	#2	#1
	Beam Spoilage	1	#2, #3	N/A	N/A	N/A	N/A	N/A

5.3.2 *Top Designs for $(S_i)_{min}$*

The top score achieved for $(S_i)_{min}$ was 10, and the highest parameter value achieved was -86.08 dBm. Using equations (3-2), (3-10), and (3-17) this $(S_i)_{min}$ corresponds to a W_i of -47.64 dBm, or 1.75×10^{-8} watts. Many designs achieved both the top score and the parameter value.

The key components, ones that did not vary amongst designs, as explained in section 5.3, for the designs achieving top performance for $(S_i)_{min}$ were phase shifter choice #3, first stage of low noise amplifiers choice #1, second stage of low noise amplifiers choice #2, third stage of low noise amplifiers choice #1, and low noise amplifier placement choice #1. The key components are summarized in Table 5-5.

As discussed in section 5.2.2 the trait PS choice #3, LNA1 choice #1, and LNA placement choice #1 had that impacted $(S_i)_{min}$ was their improvement to the system noise figure. PS choice #3, LNA1 choice #1, and LNA3 choice #1 had lower individual F than the other choices for those components. And by placing the first stage of low noise amplifiers upfront in the receive chain, LNA placement choice #1, a less noisy component was first thus lowering the overall system F.

5.3.3 *Top Designs for SFDR*

The top score achieved for *SFDR* was 2.2775, and the highest parameter value achieved was 29.7033 dB. Several designs achieved both the top score and parameter value.

The key components for the designs achieving top performance for *SFDR* were the number of elements per sub-array, first stage of low noise amplifiers choice #2,

second stage of low noise amplifiers choice #1, and third stage of low noise amplifiers choice #2. The key components are summarized in Table 5-5.

The biggest impact these components/architecture had was that their effect on lowering the system gain, as discussed in section 5.2.3. All these low noise amplifier choices offered lower individual gain than the other choices. The choice of one element per sub-array lowered the overall gain by not using a power combiner, thus not multiplying the gain by *M*. Placement of the first stage of low noise amplifiers upfront increases gain upfront in the receive chain, but lowers the gain late in the system, which had an impact on *I*, as discussed in section 5.2.3.

5.3.4 *Top Designs for Cost*

The top score achieved for cost was 10, and the top parameter value achieved was $4497.00. Several designs achieved both the score and the parameter value.

The key components for the designs achieving top performance for cost were elements per sub-array, phase shifter choice #2, first stage of low noise amplifiers choice #2, third stage of low noise amplifiers choice #2, analog-to-digital converter choice #1, and low noise amplifier placement choice #2. The key components are listed in Table 5-5.

All of these choices caused a lowering of the total system cost, as discussed in section 5.2.4. Phase shifter choice #2, first stage of low noise amplifiers choice #2, third stage of low noise amplifiers choice #2, and analog-to-digital converter choice #1 all had significantly lower individual costs than other choices. Having eight elements per sub-array significantly lowers the cost by lowering the number of components used in the system, 32/*M*, for components after the sub-arraying. Low noise amplifier placement

choice #2 lowers the system cost by lowering number of LNAs needed by placing them after the sub-arrays (32/*M*).

5.3.5 *Top Designs for Mass*

The top score for the output parameter mass was 10, and the best value was 523.6032 grams. Many designs achieved both the top score and parameter value.

The key components for the designs achieving top performance for mass were elements per sub-array, phase shifter choice #1, the first stage of low noise amplifiers choice #1, and the third stage of low noise amplifiers choice #1. These components are listed in Table 5-5.

As discussed in section 5.2.5 all these key components caused a decrease in the overall system mass. Phase shifter choice #1, first stage of low noise amplifiers choice #1, and third stage of low noise amplifiers choice #1 all had significant lower individual mass than their other choices. Even though having only one element per sub-array increased the number of individual components of the system, this was more than offset by the increase in individual mass of the power combiners needed for multiple elements per sub-array, so using one element per sub-array actually lowered the system mass.

5.3.6 *Top Designs for Power Consumption*

The top score achieved for power consumption was 10, and the top parameter value was 35.2960 watts. Several designs achieved both the top score and parameter value.

The key components of designs with the best performance for power consumption were eight elements per sub-array, phase shifter choice #2, first stage of low noise amplifiers choice #1, third stage of low noise amplifiers choice #1, analog-to-digital

converter choice #1, and low noise amplifier placement choice #2. These choices are summarized in Table 5-5.

All of these component/architecture choices helped reduce the overall system power, as discussed in section 5.2.6. Phase shifter choice #2, first stage of low noise amplifiers choice #1, third stage of low noise amplifiers choice #1, and analog-to-digital converter choice #1 all had lower individual power consumption than other corresponding choices. Using eight elements per sub-array dramatically reduced the system power consumption by reducing the total number of RF components needed ($32/M$) after the sub-arraying. Low noise amplifier placement choice #2 reduced the number of LNAs needed by placing them after the sub-arraying, thus reducing system power.

5.3.7 *Top Designs for Beam Spoilage*

The top score for beam spoilage was 9.8817, the top parameter value for change in beam width ratio was 0, the top parameter value for change in gain of the main beam was 0, the top value for change in beam pointing angle ratio was 0.0355.

The key architecture of these designs was having one element per sub-array, as the number of elements per sub-array impacted the radiation patterns of the array. The choice of phase shifter did affect the beam spoilage performance, as was discussed in section 5.2.7, but did not outweigh the effect of the number of elements per sub-array as all designs with one element per sub-array out performed designs with multiple elements per sub-array.

5.4 *Best Overall Design*

The final output analyzed was which design had the maximum overall score. This determination for best overall design was based on the total of the individual output parameter scores. The best designs based on a particular output parameter were discussed in section 5.3 above.

Eight designs tied for having the best overall design score. The scores for the individual output parameters as well as the overall score for these designs are listed in Table 5-6.

These eight designs were further narrowed to the top four designs by considering the actual parameter values of the designs, specifically where the designs reached maximum and minimum scores. The designs achieved the maximum score for the output parameter $(S_i)_{min}$ and the minimum score for *SFDR*. For those output parameters there were differences in the actual values that did not reflect in the scores because they were all outside either the maximum threshold for $(S_i)_{min}$, or the minimum threshold for *SFDR*. The eight top scoring designs could further be broken up into two groups of four designs when considering output parameter values. Table 5-7 lists the output parameter values corresponding to the designs of group A and group B. The only two differing values are for $(S_i)_{min}$ and *SFDR*, and the difference between *SFDR* is much more significant. Therefore the designs of group A were deemed the best designs overall due to their performance in *SFDR*. Design #2113 was selected arbitrarily amongst these designs to be the reference design used in the calculations of section 5.2 and 5.3.

Table 5-6 Total and output parameter ***scores*** for top designs

	Output Parameters						
	$(S_i)_{min}$	SFDR	Cost	Mass	Power	Beam Spoilage	Total
Scores	10	0	8.3743	4.5601	7.7178	9.8721	40.5243

Table 5-7 Output parameter ***values*** of top design groups

			Output Parameters							
			$(S_i)_{min}$	SFDR	Cost	Mass	Power	Δbw ratio	Δgain	Δangle ratio
Group	A	**Values**	-86.0802	10.8128	7156.04	697.876	89.928	0.0004	0.0034	0.0364
	B		-86.0813	6.1536	7156.04	697.876	89.928	0.0004	0.0034	0.0364

Table 5-8 Component/Architecture choices of top designs

	Component/Architecture								
	Elements/sub-array	PS choice	LNA1 choice	BPF choice	LNA2 choice	LPF choice	LNA3 choice	A/D choice	LNA placement choice
Choice	8	#3	#1	Any	#1	Any	#1	#1	#1

The component/architecture choices of design group A are listed in Table 5-8. For several components the choice of component was irrelevant to the score of the designs, as the choice of component changed from design to design without affecting the outcome, these components were the choice of band pass filters, and choice of low pass filters. The choices that did impact the performance were the choice of the number of elements per sub-array, the choice of phase shifter, the choice of the first stage of low noise amplifiers, choice of the second stage of low noise amplifiers, choice of the third stage of low noise amplifiers, choice of analog-to-digital converter, and choice of the placement of the first stage of low-noise amplifiers. The choice of the second stage of low noise amplifiers was the difference between design groups A and B.

As can be seen from Table 5-6, and Table 5-7 the top designs performed exceptionally well for the output parameters $(S_i)_{min}$ and beam spoilage, very well for cost and power performance, slightly poor in total mass, and extremely poor in SFDR. If a user would want better performance from some of the weaker performing output parameter then a design from section 5.2 or 5.3 could be selected.

5.5 *Chapter Summary*

Several trends were examined in this chapter. The first trend examined was the input parameters that had the greatest impact on each output parameter. The results were presented in Table 5-2, Table 5-3, and Table 5-4. Another trend examined was the design(s) that showed the best performance for a particular output parameter. This result was summarized in Table 5-5. Finally the design(s) that had the best overall score and what input parameters/components/architecture that design(s) had were presented in Table 5-6, Table 5-7, and Table 5-8. In the next chapter a summary of the research results and analysis, as well as recommendations for future work are presented.

Chapter 6. Conclusions And Recommendations

6.1 *Introduction*

Chapter 6 provides a summary of the research results and analysis. Recommendations for future research are provided as well.

6.2 *Restatement of Research Goal*

As stated in Sections 1.1 and 1.2, the research goals were:

1. To provide trade space analysis of differing antenna array architectures and associated RF components using system-modeling tools.
2. To develop an accompanying system modeling tool to allow users to tailor fit their design considerations when performing analysis on a system of their own specifications.

6.3 *Conclusions*

Eight designs tied for the overall top score based on a summation of the 6 output parameter scores. These eight designs were further narrowed down to four designs by considering the output parameter values for the two parameters where the designs either achieve maximum or minimum scores, thus their performance varied amongst these two output parameters $(S_i)_{min}$ and *SFDR*. The performance of these four designs is discussed in section 5.4, and *SFDR* performance was the deciding factor separating the designs.

The four best designs contained the following key components/architecture choices eight elements per sub-array, phase shifter choice #3, first stage of low noise amplifiers choice #1, second stage of low noise amplifiers choice #1, third stage of low noise amplifiers choice #1, analog-to-digital converter choice #1, placement of the first stage of low-noise amplifiers choice #1. Table 5-8 lists the components/architecture choices of the top designs.

The designs with the top overall design score performed exceptionally well in the output parameters $(S_i)_{min}$ and beam spoilage, very well in cost and power performance, slightly poor in total mass, and extremely poor in *SFDR*. Table 5-6, and Table 5-7 show the performance of the top designs.

6.4 *Significant Research Contributions*

This research has met the two stated design goals. First a detailed trade space analysis was performed, with the results presented in three different formats as detailed in sections 5.2, 5.3, and 5.4. Factors contributing to the performance of each specific output parameter were determined, the best possible design choices based on the current range of components used in the study were determined for each particular output parameter, as well as the best overall design based on specifications set forth for this design, and these determinations can be used as a future reference when designing follow on systems. Also, a system modeling tool was developed using Matlab® which can be used for follow on analysis and design, and can be updated with additional choices of system components for use to meet other applications.

6.5 *Recommendations for Future Work*

One option for future work would be to further improve the spurious free dynamic range of the system. One limitation that stood out in this study was the failure of a large number of designs to meet the spurious free dynamic range goals set forth. The cause appeared to be too much gain in the system. One remedy would be to reduce the gain of the low noise amplifiers chosen for the study. Another would be to replace the three stages of low noise amplifiers with two stages, preferably one stage as the first component in the receive chain and another stage directly before the analog-to-digital converters. A final possibility would be to explore the option of using automatic gain control amplifiers as components in the system.

Another possible follow-on activity would be to update the system modeling tools used in the course of this study to be more user friendly. This update could be done by allowing user input outside of the code, most likely by graphical user interface (GUI). An experienced coder could modify the current modeling tools to allow for a GUI interface, thus improving user involvement.

Appendix A: List of Components with Specifications

List of Components with specifications										
	Manufacture	**Model #**	**Freq. Range**	**G**	**F**	**I**	**Cost**	**Mass**	**Power**	**Bits**
			(GHz)	**(dB)**	**(dB)**	**(dB)**	**($)**	**(g)**	**(W)**	**(#)**
Low Noise Amp 1st Stage										
Choice #1	TriQuint	TGA8399B-scc	6 to 13	26	1.5	21	52	0.005	1.95	
Choice #2	TriQuint	TGA1342-scc	2 to 20	9	3.5	27.5	38	0.0075	2.16	
Phase Shifter										
Choice #1	TriQuint	TGP6336-eeu	6 to 18	-9	9	100	99	0.0062	0.22	5
Choice #2	Bookham	P35-4400-00-200	8 to 11	-9	9	100	50	0.007	0.0005	6
Choice #3	Northrup/ Grumman	XB-PHS-S1145-A	8 to 12	-5	5	100	84	0.0097	0.0015	6
Mixer 1										
	TriQuint	TGC1452-EPU	.2 to 18	12	12.5	7.7	16	0.0007	0.64	
Band Pass Filter										
Choice #1	Mini-Circuits	PHP-900	.910 to 2.10	-1	1	100	11.05	5.2	0	
Choice #2	Mini-Circuits	PHP-1000	1.2 to 2	-1	1	100	11.05	5.2	0	
Low Noise Amp 2nd Stage										
Choice #1	TriQuint	TQ3631	1.81 to 2.17	13	1.5	10	50	1	0.5	
Choice #2	Macom	MAAM 12031	1.7 to 2.0	20	1.65	17	50	1	0.5	

	Manufacture	Model #	Freq. Range (GHz)	G (dB)	F (dB)	I (dB)	Cost ($)	Mass (g)	Power (W)	Bits (#)
Mixer 2										
	TriQuint	TGC1452-EPU	.2 to 18	12	12.5	7.7	16	0.0007	0.64	
Low Pass Filter										
Choice #1	Mini-Circuits	PLP-300	0 to .270	-1	1	100	8.45	5.2	0	
	Mini-Circuits	PLP-450	0 to .400	-1	1	100	8.45	5.2	0	
Low Noise Amp 3rd Stage										
Choice #1	Macom	A-75-3	.010 to .500	21	1.7	16	50	1	0.21	
Choice #2	Mini-Circuits	Amp-75	.005 to .500	19	2.4	28	35.23	1.5	0.435	
Power Combiner										
2 elements per sub-array	Pulsar Microwave	PS2-16-450/8S	8 to 12.4	0.4			200	18	0	
4 elements per sub-array	Pulsar Microwave	PS4-12-452/7S	8 to 12.4	0.8			225	116	0	
8 elements per sub-array	Pulsar Microwave	PS8-11-454/4S	8 to 14.0	1.3			400	158	0	
Analog to Digital Converter										
Choice #1	Maxim	MAX106	(600 MSps)				149.5	3.95	4.88	8
Choice #2	Maxim	MAX104	(1000 MSps)				398.7	3.95	5	8
Choice #3	Maxim	MAX108	(1500 MSps)				495	3.95	5.2	8

Appendix B: Development of *F* and *I* Equations for Components in Parallel

Introduction

In this appendix, the equations used to determine noise figure and third-order intercept point for components in parallel are developed. While equations for use with components in series are readily available, no published results were found for the parallel component case. To develop the equations needed, I consulted with Mr. James Theimer of AFLR/SNDM at Wright-Patterson AFB, OH.

To develop noise figure and third-order intercept point equations for use in the case of parallel components, the signal and noise power in a power combiner were examined. In general, signals in phase add constructively and signals out of phase add destructively. It was assumed that the input signals to the receive chain were in phase and the noise at the input was random and out of phase.

Signal Power Development

To begin, the signal power was examined. A signal can be represented as

$$V_k(t) = a_k\left[\cos(\omega t + \theta_k) + j\sin(\omega t + \theta_k)\right] = a_k e^{j(\theta_k + \omega t)} \qquad \text{(B-1)}$$

where a represents the amplitude of the signal, k represents the inputs of n channels into a power combiner ($k = 1,2,\ldots n$), ω is the angular frequency term, t is the time variable, the phase (θ_k) is assumed the same for all channels and is considered a uniformly distributed variable from π to $-\pi$. If the power combiner adds n identical signals, let the sum of the n channels equal

$$V(t) = \sum_{k=1}^{n} V_k(t) = \sum_{k=1}^{n} a_k \left[\cos(\omega t + \theta_k) + j\sin(\omega t + \theta_k)\right] = \sum_{k=1}^{n} a_k e^{j(\theta_k + \omega t)} = nae^{j(\theta + \omega t)} \quad \text{(B-2)}$$

and the expected value of *V(t)* is found to be

$$\begin{aligned} \mathrm{E}[V(t)] &= \mathrm{E}\left[nae^{j(\theta+\omega t)}\right] = \int_{-\pi}^{\pi} nae^{j(\theta+\omega t)} f_x(\theta) d\theta = e^{j\omega t} \int_{-\pi}^{\pi} nae^{j\theta} \frac{1}{2\pi} d\theta \\ &= (e^{j\omega t}) \frac{na}{2\pi} e^{j\theta} \Big|_{-\pi}^{\pi} = 0 \end{aligned} \quad \text{(B-3)}$$

where $f_x(\theta)$ is the probability density function for a uniform random variable, in this case distributed from $-\pi$ to π. The time average, power per one ohm (Ω), is found to be

$$V(t)V(t)^* = nae^{j(\theta+\omega t)}(na^* e^{-j(\theta+\omega t)}) = n^2 aa^* e^{j(\theta+\omega t)} e^{-j(\theta+\omega t)} = n^2 |a|^2 \quad \text{(B-4)}$$

and the mean of the time average is found to be

$$\mathrm{E}\left[V(t)V(t)^*\right] = \mathrm{E}\left[n^2|a|^2\right] = n^2 \mathrm{E}\left[|a|^2\right] = n^2 |A_o|^2 \quad \text{(B-5)}$$

where A_o is an arbitrary amplitude for the signal. The mean of the time average is also the equal to the variance of *V(t)* because

$$Variance[V(t)] = \mathrm{E}\left(|V(t)|^2\right) - \left(\mathrm{E}[V(t)]\right)^2 = \mathrm{E}\left(|V(t)|^2\right) - 0 = \mathrm{E}\left[V(t)V(t)^*\right] \quad \text{(B-6)}$$

(Theimer, 2003).

Noise Power Development

Next the noise power was examined. A noise signal can be represented as

$$V_k(t) = a_k \left[\cos(\omega t + \theta_k) + j\sin(\omega t + \theta_k)\right] = a_k e^{j(\theta_k + \omega t)} \quad \text{(B-7)}$$

where *a* represents the amplitude of the signal, *k* represents the inputs of *n* channels into a power combiner (k=1,2,…n), ω is the angular frequency term, *t* is the time variable, the

phase (θ_k) is assumed uniformly distributed from $-\pi$ to π, the noise signals are assumed to be independent and identically distributed, and the amplitude is assumed independent of the phase. If the power combiner adds *n* unequal noise signals, let the sum of the *n* channels equal

$$V(t) = \sum_{k=1}^{n} V_k(t) = \sum_{k=1}^{n} a_k \left[\cos(\omega t + \theta_k) + j \sin(\omega t + \theta_k)\right] = \sum_{k=1}^{n} a_k e^{j(\theta_k + \omega t)} \tag{B-8}$$

and the expected value of *V(t)* is found to be

$$\begin{aligned} \mathrm{E}[V(t)] &= \mathrm{E}\left[n a_k e^{j(\theta_k + \omega t)}\right] = \int_{-\pi}^{\pi} n a_k e^{j(\theta_k + \omega t)} f_x(\theta_k) d\theta_k = e^{j\omega t} \int_{-\pi}^{\pi} n a_k e^{j\theta_k} \frac{1}{2\pi} d\theta_k \\ &= (e^{j\omega t}) \frac{n a_k}{2\pi} e^{j\theta_k} \Big|_{-\pi}^{\pi} = 0 \end{aligned} \tag{B-9}$$

where $f_x(\theta_k)$ is the probability density function for a uniform random variable, in this case distributed from $-\pi$ to π. The time average, power per one Ω, is found to be

$$V(t)V(t)^* = \left(\sum_{k=1}^{n} a_k e^{j(\theta_k + \omega t)}\right)\left(\sum_{l=1}^{n} a_l{}^* e^{-j(\theta_l + \omega t)}\right) = \sum_{k=1}^{n}\sum_{l=1}^{n} a_k a_l{}^* e^{j\theta_k} e^{-j\theta_l} \tag{B-10}$$

and the mean of the time average is found to be

$$\mathrm{E}\left[V(t)V(t)^*\right] = \mathrm{E}\left[\sum_{k=1}^{n}\sum_{l=1}^{n} a_k a_l{}^* e^{j\theta_k} e^{-j\theta_l}\right] = \sum_{k=1}^{n}\sum_{l=1}^{n} \mathrm{E}\left[a_k a_l{}^*\right] \mathrm{E}\left[e^{j\theta_k} e^{-j\theta_l}\right] \tag{B-11}$$

assuming the amplitude and phase of the noise signals are independent. For $E(a_k a_l{}^*)$ there are two cases:

1. When k = l, then

$$\mathrm{E}\left[a_k a_l{}^*\right] = \mathrm{E}\left[|a_k|^2\right] = |A|^2 \tag{B-12}$$

where A is an arbitrary amplitude of the noise signal.

2. When $k \neq l$, then

$$\mathrm{E}\left[a_k a_l^{*}\right] = \mathrm{E}[a_k]\mathrm{E}\left[a_l^{*}\right] = A_k A_l \tag{B-13}$$

For E($e^{j\theta_k} e^{j\theta_l}$) there are two cases:

1. When $k = l$, then

$$\mathrm{E}\left[e^{j\theta_k} e^{-j\theta_l}\right] = \mathrm{E}\left[e^{j\theta_k} e^{-j\theta_{kl}}\right] = \mathrm{E}[e^0] = 1 \tag{B-14}$$

2. When $k \neq l$, then

$$\mathrm{E}\left[e^{j\theta_k} e^{-j\theta_l}\right] = \mathrm{E}[e^{j\theta_k}]\mathrm{E}[e^{-j\theta_l}] = 0 \tag{B-15}$$

Thus,

$$\mathrm{E}\left[V(t)V(t)^{*}\right] = \sum_{k=1}^{n} \mathrm{E}\left[\left|a_k\right|^2\right]\mathrm{E}\left[e^{j\theta_k} e^{-j\theta_k}\right] = \sum_{k=1}^{n} |A|^2 = n|A|^2 \tag{B-16}$$

using Equation (B-12) and (B-14). (Theimer, 2003).

Signal-to-Noise Ratio and Noise Figure Development

The ratio of power of the summed signals to the power of the summed noise signals is,

$$Signal/Noise = \frac{n^2|A_o|^2}{n|A|^2} = \frac{n|A_o|^2}{|A|^2} \tag{B-17}$$

And the noise figure improvement is

$$F = \frac{\frac{S_i}{N_i}}{\frac{S_o}{N_o}} = \frac{\frac{S_i}{N_i}}{\frac{nS_i}{N_i}} = \frac{1}{n} \tag{B-18}$$

where S_i/N_i is the signal to noise ratio into the power combiner, and S_o/N_o is the signal to noise ratio out of the power combiner. Thus the noise figure of the system is reduced by

a factor of 1/*n*, where *n* is the number of input ports to the power combiner. This reduction assumes no additional noise added by the power combiner.

This noise figure found at this point is for the path of a single element. To get the noise figure at the sub-array level the noise figure found in Equation (B-18) must be multiplied by *n*, the number of input ports. This form of noise figure is consistent with the radar range equation where the gain of the antenna is tracked separately, and keeps the noise figure found by using (B-18) from falling below thermal noise level which would be unrealistic. (Theimer, 2003).

Third-order Intercept Point Development

A similar development can be made for the improvement of the third-order intercept point. The power out of an amplifier is

$$P_{oamp} = GP_{iamp} + AP^3{}_{iamp} \tag{B-19}$$

where P_{oamp} is the power out of the amplifier, G is the amplifier gain, P_{iamp} is the power into the amplifier, A is constant for the third-order response.

The input third-order intercept point (*IIP3)* is the power where the linear and third-order outputs are equivalent,

$$GIIP3 = AIIP3^3 \tag{B-20}$$

thus,

$$IIP3 = \sqrt{\frac{G}{A}} \tag{B-21}$$

The output third-order intercept point (*OIP3*) is then

$$OIP3 = G(IIP3) \tag{B-22}$$

For parallel components, where identical amplifiers are fed into a power combiner, the *IIP3* will not change from what was found in Equation (B-21). The *OIP3* does change due to the power combining and becomes.

$$OIP3_n = nG(IIP3) = n(OIP3) \tag{B-23}$$

where $OIP3_n$ denotes the output third-order intercept point for a n input power combiner, and n is the number of inputs to the power combiner.

As stated above for the noise figure, so far this only takes into account the effect at the element level for input power. To take into account the gain of the antenna, or sub-array level for the purposes of this study, a different case must be examined. Here the power into the amp is

$$P_{iamp} = P_{in} \Big/ n \tag{B-24}$$

where P_{in} is the power into the sub-array, as the power is split into n paths. And the IIP3 for each amplifier becomes

$$\frac{G}{n} IIP3_n = A\left(\frac{IIP3_n}{n}\right)^3 \tag{B-25}$$

And the $IIP3_n$ is

$$IIP3_n = n\sqrt{\frac{G}{A}} = n(IIP3) \tag{B-26}$$

And the $OIP3_n$ after power combining becomes

$$OIP3_n = n^2 G(IIP3) = n^2 (OIP3) \tag{B-27}$$

(Theimer, 2003).

Bibliography

Balanis, Constantine A. *Antenna Theory (2nd Edition).* New York:John Wiley and Sons, Inc., 1997.

Bucciarelli, Tullio, Giovanni Picardi. "The A/D Conversion Errors Analysis in Digital Beam Forming", *Proceedings of EUSIPCO-88, Fourth European Signal Processing Conference, Grenoble, France. 7*87-790. New York: North-Holland, 1988.

Chiba, I., R. Miura, T. Tanaka, Karasawa Y. "Digital Beam Forming (DBF) Antenna System for Mobile Communications", *IEEE Aerospace and Electronics Systems Magazine* v12:n9: 31-41(Sept 1997).

Curtis, David. Sensors Directorate, Air Force Research Lab (AFRL/SNHA), Hanscomb Air Force Base MA. Personal correspondence and antenna array evaluation code. April 2002.

Eagleware® Corporation. Excerpts from website and help menus of software. www.eagleware.com. 11 Feb 04.

Gonzalez, Guillermo. *Microwave Transistor Amplifiers analysis and design.* New Jersey:Prentice-Hall Inc, 1984.

Gupta, S., A. Kumar. "Multilayer Planar Array Radiators Compatible with Digital Beam Forming Arrays", *Indian Journal of Physics, Part B*, v75b:n3 (June 2001).

Horton, Charles R., Kenneth Abend. "Adaptive Array Antenna for Satellite Cellular and Direct Broadcast Communications", *JPL, Proceedings of the Third International Mobile Satellite Conference.* 47-52 (Jan 93)

Litva, John, Titus K-Y Lo. *Digital Beamforming in Wireless Communications*. Boston:Artech House, 1996.

McCord, James E. *A Survey of Digital Beamforming Techniques and Current Technology,* MS thesis, AFIT/CI/NR 88-81, Mississippi State University, 1988 (ADA196376).

Pozar, David M. *Microwave and RF Design of Wireless Systems.* New York:John Wiley and Sons, Inc, 2001.

Skolnik, Merrill I. *Introduction to Radar Systems(3rd Edition).* Boston:McGraw Hill, 2001.

Steyskal, Hans. “Digital Beamforming Antennas an Introduction”, *Microwave Journal* v30:n1: 107-122 (Jan 1987).

Steyskal, Hans. “Digital Beamforming at Rome Laboratory”, *Microwave Journal* v39:n2: 100-126 (Feb 1996).

Stutzman, Warren L., Gary A. Theile. *Antenna Theory and Design (2nd Edition).* New York:John Wiley and Sons, Inc., 1998.

Tanaka, Toyohisa, Ryu Miura, Isamu Chiba, Yoshio Karasawa. “An Application Specific Integrated Circuit Implementation of a Digital Beam-Forming Multibeam Antenna”, *Electronics and Communications in Japan, Part I* V80:n2: 100-111 (1997).

Theimer, James P. Sensors Directorate, Air Force Research Lab (AFRL/SNDM), Wright-Patterson Air Force Base OH. Personal correspondence. June 2003.

Tsui, James. *Digital Techniques for Wideband Receivers.* Boston:Artech House, 2001.

Vendelin, George D., Anthony M. Pavio, Ulrich L. Rohde. *Microwave Circuit Design Using Linear and Nonlinear Techniques.* New York:John Wiley and Sons, Inc., 1990.

Vizmuller, Peter. *RF Design Guide systems, circuit, and Equations.* Boston:Artech, 1995.

REPORT DOCUMENTATION PAGE

Form Approved
OMB No. 074-0188

PLEASE DO NOT RETURN YOUR FORM TO THE ABOVE ADDRESS.

1. REPORT DATE *(DD-MM-YYYY)*	**2. REPORT TYPE**	**3. DATES COVERED** *(From – To)*
21-12-2004	**Master's Thesis**	June 2002 – Dec 2004

4. TITLE AND SUBTITLE

TRADE SPACE ANALYSIS OF ANTENNA ARRAY ARCHITECTURE USING SYSTEM MODELING TOOLS

5a. CONTRACT NUMBER

5b. GRANT NUMBER

5c. PROGRAM ELEMENT NUMBER

6. AUTHOR(S)

Johnson, Eugene, 1Lt, USAF

5d. PROJECT NUMBER

5e. TASK NUMBER

5f. WORK UNIT NUMBER

7. PERFORMING ORGANIZATION NAMES(S) AND ADDRESS(S)

Air Force Institute of Technology
Graduate School of Engineering and Management (AFIT/EN)
2950 Hobson Way
WPAFB OH 45433-7765

8. PERFORMING ORGANIZATION REPORT NUMBER

AFIT/GE/ENG/04-26

9. SPONSORING/MONITORING AGENCY NAME(S) AND ADDRESS(ES)

AFRL/VSSE
Attn: Mr. Kevin V. Sickles
2241 Avionics Circle, Bldg 620
WPAFB OH 45433-7765 DSN: 785-4120, ext4224

10. SPONSOR/MONITOR'S ACRONYM(S)

11. SPONSOR/MONITOR'S REPORT NUMBER(S)

12. DISTRIBUTION/AVAILABILITY STATEMENT

APPROVED FOR PUBLIC RELEASE; DISTRIBUTION UNLIMITED.

13. SUPPLEMENTARY NOTES

14. ABSTRACT

This trade study has two objectives. The first provides a trade space analysis of differing array architectures and associated radio frequency components using system-modeling tools. The second objective develops system modeling tools aiding similar analysis by other users. These objectives were accomplished by evaluating a selected group of output parameters to include overall system cost, mass, and power consumption, as well as the minimum detectable input level, system spurious free dynamic range, and selected beam spoilage parameters caused by the use of discrete phase shifters. A fixed number of designs were evaluated using simulation. The evaluation process examined input parameter and design impact on the output parameters and overall best design. The best overall design, by score, performed exceptionally well for minimum detectable input level and beam spoilage parameters, very well for cost and power performance, and poor for total mass and spurious free dynamic range. The best overall design offered a 97% improvement in evaluation score over the lowest scoring design. The placement of the first stage of low noise amplifiers within the RF component chain, as well as the number of sub-arrays, were among the design parameters found to have the most profound affect on the output results. These results match commonly accepted guidelines in radar design. Selected portions of this study were verified and compared to results from commercially available software, GENESYS® by Eagleware Corporation.

15. SUBJECT TERMS

Antenna Arrays; Tradeoff Analysis; Antenna Components; Radiofrequency; Low Noise Amplifiers

16. SECURITY CLASSIFICATION OF:			**17. LIMITATION OF ABSTRACT**	**18. NUMBER OF PAGES**	**19a. NAME OF RESPONSIBLE PERSON**
REPORT	**ABSTRACT**	**c. THIS PAGE**			Todd B. Hale, Maj, USAF (ENG)
U	**U**	**U**	**UU**	110	**19b. TELEPHONE NUMBER** *(Include area code)* (937) 255-3636, ext4639 ; e-mail: todd.hale@afit.edu

Standard Form 298 (Rev: 8-98)
Prescribed by ANSI Std. Z39-18